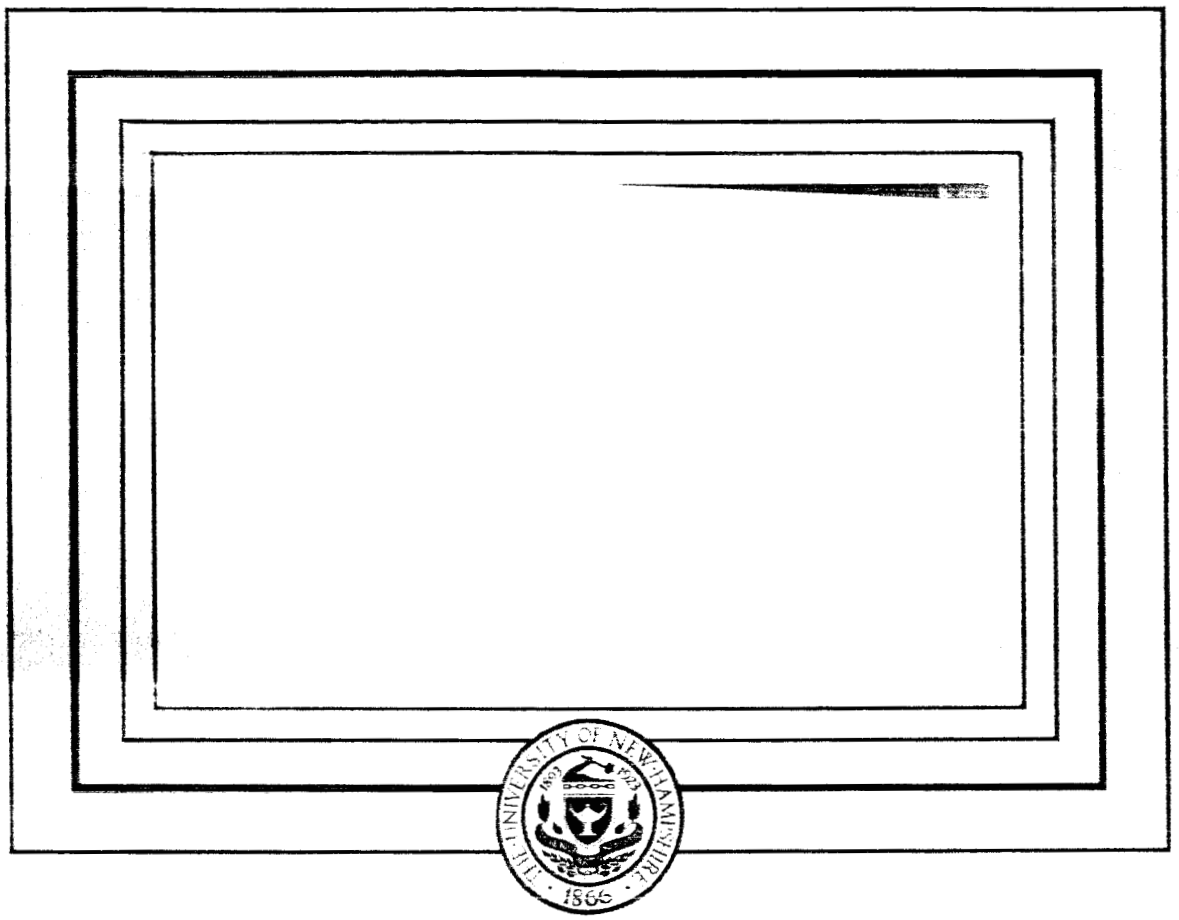

Department of Physics

UNIVERSITY OF NEW HAMPSHIRE

Durham

Design of a Neutron Monitor for Measurements in Space

J. A. Lockwood
and
L. A. Friling

NASr-164

Scientific Report No. 1

This report has been prepared for the Grants and Research Contracts Division, Office of Space Science and Applications, National Aeronautics and Space Administration.

ABSTRACT

10044

A study has been made of suitable neutron detecting systems for space measurements. As a result of this investigation a neutron monitor, consisting of a He^3 proportional counter encased in a polyethylene moderator which, in turn, is surrounded by charged particle counters, has been constructed and tested. The efficiency of this neutron detector system is 2.0 counts/neutron/cm^2 for 14 MeV neutrons and 20 cts/n/cm^2 at thermal energies. The electronics system is designed to reject neutron events occurring within 200 microseconds after a charged particle counter is triggered, thereby providing discrimination against neutron production in the detector.

A Li^6I scintillator encased in a plastic scintillator which acts as both a moderator for the neutrons and a charged particle detector has also been built and tested. This detector system was not adopted now as "space neutron monitor" because pulse shaping circuits were required and the rejection of gamma ray events was not as good as for the He^3 detector system. Studies have also been made of detectors for fast neutron measurements and directional neutron fluxes.

Acknowledgments

This research was supported by the National Aeronautics and Space Administration under contract NASr-164. We appreciate the many helpful discussions with Drs. E. L. Chupp and J. H. Trainor. The assistance of Robert Colburn, David Forrest and Richard St. Onge for the development and preliminary evaluation of the Li^6I phoswich, the directional neutron detector and the fast neutron detector is acknowledged.

Table of Contents

Figure Captions

Figure 1 - Neutron energy dependence of the reaction cross-sections for He^3, B^{10}, and Li^6.

Figure 2 - Pulse height spectrum for $B^{10}F_3$ proportional counter

Figure 3 - Pulse height spectrum for 4 atm He^3 proportional counter

Figure 4 - Pulse height spectrum for 10 atm He^3 proportional counter

Figure 5 - Pulse height spectrum for Li^6I neutron scintillator

Figure 6 - Pulse height spectrum for NE421 (Li^6ZnS) neutron scintillator

Figure 7 - Experimental layout for calibration of neutron monitors using the 400 KeV Van de Graaff accelerator

Figure 8 - Cross-section of neutron collimator used with the Van de Graaff accelerator

Figure 9 - Angular dependence of the fast neutron flux with the collimator (Figure 8)

Figure 10 - Associated particle detector assembly used with the He^3 target in accelerator

Figure 11 - Cross-section of the tube module in the neutron detector

Figure 12 - Schematic diagram of the electronics for the prototype neutron detector

Figure 13 - Completed prototype of neutron detector system

Figure 14 - View of the interior of the prototype neutron detector with a logic and a scaler board removed

Figure 15 - Efficiency of the neutron detector as a function of neutron energy

Figure 16 - Schematic diagram of the experimental layout to measure the angular dependence of the efficiency of the neutron detector

Figure 17 - Angular dependence of the efficiency of the prototype

Figure 18a- Pulse height distributions for D-D neutrons on a stilbene scintillator without pulse shaping

Figure Captions (Continued)

Figure 18b - Pulse height distribution for D-D neutrons on a stilbene scintillator with pulse shaping

Figures A-1 thru A-6 - Schematic diagrams of electronic circuits for neutron detecting system

Figure B1 - Schematic diagram of the Li^6I phoswich assembly

Figure B2 - Circuit diagram for the pulse shape discriminator used in phoswich assembly (Peterson and Nitardy, 1961).

Figure B3 - Pulse height spectra (ungated) for 3 Mev neutrons on the Pilot B and LiI scintillators and the phoswich assembly

Figure B4 - Pulse height spectra (gated) for 3 Mev neutrons on the Pilot B and LiI scintillators and the phoswich assembly

Figure B5 - Pulse height spectra (ungated) for 14 Mev neutrons on the Pilot B and LiI scintillators and the phoswich assembly

Figure B6 - Pulse height spectra (gated) for 14 Mev neutrons on the Pilot B and LiI scintillators and the phoswich assembly

List of Tables

Design of a Neutron Monitor for Measurements in Space

J. A. Lockwood

and

L. A. Friling

Physics Department, University of New Hampshire,
Durham, New Hampshire

I. Introduction

A study has been made of different types of neutron detector systems for measurements of the total neutron intensity both near and far from the earth. Such a neutron detection system will be referred to as a "space neutron monitor" because, in general, some moderating material will surround the neutron detector itself and charged particle detectors will be required to discriminate against neutron production in the monitor. The design and testing of such a neutron space monitor to measure the integrated neutron flux up to about 10 Mev has been the principle concern of this investigation. Preliminary studies have also been made of detectors to measure the energy spectrum and directional intensity of the neutron flux above the atmosphere with $0.1 < E_n < 10$ Mev.

In the vicinity of the earth, but above the earth's atmosphere, the monitor will measure the neutron leakage flux resulting from neutron production in the atmosphere of the earth by the normal primary cosmic radiation. On many occasions, after large solar flares, there may be an enhanced neutron leakage flux as a result of neutron

production in the atmosphere by solar protons and alphas. For most solar events such production would be confined to regions near the geomagnetic poles. On very rare occasions, such as after the 15 November 1960 solar flare, in which energetic protons ($E_p \geq 5$ Bev) were produced, neutrons may be observed at low altitudes at lower geomagnetic latitudes.

We may speculate whether there are detectable fluxes of neutrons with $0.1 < E_n < 10$ Mev arriving at the earth directly as a result of nuclear reactions on the solar surface. It is evident that such a neutron flux would be difficult to measure in the presence of the large proton fluxes following solar flares.

At large distances from the earth, a neutron monitor would measure the neutron intensity from other sources. For example, the presence of a neutron albedo about twice that for the earth, or 0.17 $n/cm^2/sec$, has been postulated for the moon (Rao, 1963). We might expect the transit times from the sun to a space vehicle at large distances from the earth to be different for solar protons than for solar neutrons. Consequently, the nature of the solar flare mechanism and the propagation of the protons through the interplanetary field might be studied.

In addition, this neutron detection system, when flown near the earth, can indirectly monitor the intensity-time variations of the cosmic radiation because the neutron leakage flux is generically related to the primary cosmic radiation interacting with the earth's atmosphere.

For meaningful comparisons of the neutron intensity above the atmosphere and in space, a "standard" neutron detection system should be used and located in, as near as possible, similar surroundings, preferably removed from any high atomic number and hydrogenous materials. An accurate calibration must be made of the detector's energy response and absolute efficiency so that the result of different flights can be compared. We may write the counting rate of any neutron detecting system as

$$C\ (\text{sec}^{-1}) = \int_0^\infty N(E)S(E)dE,$$

where N(E) is the differential neutron energy spectrum as a function of energy and S(E) is the detector efficiency (an intrinsic property of the neutron detecting system). We can then compare theory with experiment provided S(E) is known.

In the design of this neutron detecting system, we were primarily concerned with its use to measure the neutron leakage flux near the earth, at distances of 100-500 miles. Studies of the neutron leakage resulting from the neutron production in the earth's atmosphere by galactic and solar cosmic rays are important for several reasons:

1. The albedo neutrons diffusing out of the earth's atmosphere contribute at least part of the electrons and protons trapped in the magnetosphere.

2. The capture of neutrons in atmospheric nitrogen is responsible for the production of the age-dating nuclide C^{14}, through the reaction $N^{14}(n,p)C^{14}$.

3. The generic relation of the leakage flux to lower energy portion of the cosmic radiation.

II. Survey of Neutron Measurements in Space

Investigations have been made for several years of the intensity and spectrum of neutrons in the atmosphere (Simpson, 1951; Hess et al., 1959; Bame et al., 1963), and more recently in satellites (Hess, 1960; Bame et al., 1960, 1963; Trainor, 1963). For the most part these measurements have been sporadic, having been carried out at different latitudes, altitudes, and times of the solar cycle, and generally with neutron detectors which are not directly comparable. In order to obtain a value of the neutron flux with these detectors, it is necessary to fold together the detector's energy dependent efficiency and a relative neutron spectrum. The neutron energy spectrum is not completely known and is at the present time based upon a measurement in the atmosphere (Hess et al., 1961; Newkirk, 1963; Lingenfelter, 1963). The previous work, particularly with satellite detectors, has not been sufficiently extensive and several outstanding problems remain concerning the albedo neutron flux. Some of these are:

1. Previous absolute intensity measurements are not all in agreement.
2. The latitude and longitude dependence of the total albedo neutron intensity has not been measured.
3. The angular distribution in space of the albedo neutrons is not known, nor is the energy distribution well known even at one point in space.

4. The variation with time of the total intensity in the energy spectrum is unknown, especially during solar proton events.

5. Intensity vs. distance from the earth is known only in a limited sense. No direct measurement has been made of the intensity of the energetic albedo neutrons ($E_n > 10$ Mev) which most likely contribute to energetic protons in the inner radiation belt.

The state of the art for neutron detectors for space application has not yet reached the degree of sophistication required to answer all of the above questions. However, several may be attacked by establishing a program of total intensity measurements on rockets and satellites. Thus, properly designed total neutron intensity monitors on satellites and rockets could elucidate these questions concerned with variations of the total intensity in longitude, latitude, time, and to some extent with altitude.

Space neutron detectors are generally difficult to design properly because of the problem of the production of charged particles in the detector and the vehicle carrying the detector. The problem of local production in the detector can be avoided by the use of a charged-particle counter shield around the monitor. (See Section V). The background neutron flux from the space vehicle can be evaluated by exposing the detector and the vehicle itself to a flux of energetic charged particles, or by placing the detector so that the solid angle subtended at the detector by the production source in the vehicle is minimized. In general, the latter is the desirable method. In all cases any high Z, high density material should be kept as far as possible from the detector assembly itself.

Several experimental results are now available for comparison with the neutron leakage calculations of Hess, Canfield and Lingenfelter (1961), Newkirk (1963), and Lingenfelter (1963). These results are summarized in Table I. Newkirk has calculated the neutron flux at 57° N using the S_n approximation to transport theory, while Lingenfelter has recalculated the neutron flux of Hess et al. using diffusion theory. The essential differences between the diffusion calculations are: 1) Lingenfelter has used an altitude dependence for his source function at the top of the atmosphere based upon star production measurements of Lord (1951) rather than a simple exponential, and 2) he has included the effects of inelastic scattering, thus shifting the higher energy neutrons to lower energies. The calculations of Newkirk at 57° N are in good agreement with those of Lingenfelter. Latitude variations of ~12 to 1 at solar minimum and ~7 to 1 at solar maximum are predicted by Lingenfelter, whereas Hess et al. (1961) have used the latitude dependence of the equilibrium neutron flux in the atmosphere measured by Simpson (1951) giving a latitude variation of 4.5 to 1.

In Table I the data as presented give all the current results available. Columns 2, 3, 4 and 5 give, respectively, the time of the measurement, the geomagnetic latitude, altitude and flux measured, while column 6 gives the flux corrected to 300 km using a $R^{-3.2}$ altitude variation to facilitate comparison of results. Columns 7 and 8 separate the results on the basis of whether an experimental or calculated

correction has been applied to the listed measurement to account for local production and/or charged particle response. The H or L in parentheses indicates whether the spectrum has been calculated according to the theory of Hess or Lingenfelter. Columns 9 and 10 list the calculated flux at 300 km for the two spectra.

It is at once apparent that the results separate themselves into groups. The measurements of Albert, Gilbert and Hess (1962) and Williams and Bostrom (1964) fall consistently above the calculations of Lingenfelter. However, Albert et al. measure a latitude effect of about 10 to 1, very close to that calculated by Lingenfelter. The results of Bame et al. agree well with the calculations of Lingenfelter, and the present results agree well at low latitudes. At high latitudes, Trainor and Lockwood measured a flux about 1/3 that calculated by Lingenfelter, since they find a latitude variation of $\sim$4 to 1. If these results are compared with the measurements of Bame et al. at middle latitudes, it is seen that there is good agreement between the total response of the detectors. The experimental and calculated corrections for local neutron production in Trainor and Lockwood's experiment are much larger than those estimated by Bame et al. (1963).

Summarizing, it appears that while there is some agreement between measurements and calculations, there still exist large uncertainties in the neutron albedo flux and the latitude dependence of this flux. The need for further measurements is apparent, but it is necessary that

Table I. Results of Neutron Experiments

Experiment	Year	Gmag	Altitude Km	Flux N/cm^2Sec	Flux Corrected to 300 Km N/cm^2Sec	Total Measured Flux	Gated or Corrected Flux	Calculated Flux: Hess et al.	Calculated Flux: Lingenfelter
Albert et al.,1962	1961	0°	275-1150	$.41\pm.10$	$.5\pm.12$	---	(H) $.5\pm.12$	$.36\pm.09$	$.100\pm.02$
Trainor and Lockwood						(H) $.13\pm.04$	(H) $.10\pm.03$	$.36\pm.09$	
	1962	0°	300	$.100\pm.03$ $.085\pm.03$	$.10\pm.03$ $.085\pm.03$	(L) $.11\pm.03$	(L) $.085\pm.03$		$.10\pm.02$
Bame et al. 1963	1961	8.7°	320	$.12\pm.04$	$.12\pm.04$	(H) $.12\pm.04$	---	$.37\pm.09$	$.10\pm.02$
Bame et al.						(H) $.33\pm.11$	---	$.66\pm.17$	
	1961	36.5°	650	$.28\pm.09$ $.22\pm.08$	$.33\pm.11$ $.26\pm.09$	(L) $.26\pm.09$			$.26\pm.05$
Trainor and Lockwood						(H) $.24\pm.07$	(H) $.17\pm.05$	$.66\pm.17$	
	1962	36.5°		$.17\pm.05$ $.15\pm.05$	$.17\pm.05$ $.15\pm.05$	(L) $.21\pm.06$	(L) $.15\pm.05$		$.26\pm.05$

Table I. Results of Neutron Experiments (Continued)

Experiment	Year	Gmag	Altitude Km	Flux N/cm^2Sec	Flux Corrected to 300 Km N/cm^2Sec	Total Measured Flux	Gated or Corrected Flux	Calculated Flux: Hess et al.	Calculated Flux: Lingenfelter
Williams and Bostrom 1962							(H) $2.26\pm.8$		
		40°	1000	$1.65\pm.59$	$2.26\pm.8$	---	(L)	$.77\pm.1$	$.32\pm.06$
	1962	43°	1000	$1.76\pm.77$	2.4 ± 1.0	---	2.4 ± 1.0	$.89\pm.22$	$.37\pm.07$
Bame et al. 1960	1959	44.5°	120	$.38\pm.08$	$.34\pm.07$	(L) $.34\pm.07$	---	$.93\pm.24$	$.34\pm.07$
Trainor and Lockwood						(H) $.39\pm.12$	(H) $.26\pm.08$	$1.22\pm.31$	
				$.26\pm.08$	$.26\pm.08$	(L)	(L)		
	1962	50°	300	$.22\pm.07$	$.22\pm.07$	$.33\pm.11$	$.22\pm.07$		$.57\pm.11$
Albert et al. 1962	1961	80°	275-1150	$3.2\pm.8$	3.8 ± 1.0		(H) 3.8 ± 1.0	$1.80\pm.45$	$1.15\pm.23$
Trainor and Lockwood						(H) $.6\pm.2$	(H) $.35\pm.13$	$1.80\pm.45$	
				$.35\pm.13$	$.35\pm.13$	(L)	(L)		
	1962	80°	300	$.30\pm.1$	$.3\pm.1$	$.52\pm.17$	$.3\pm.1$		$1.15\pm.23$

these measurements should provide for experimental separation of the albedo flux from that produced locally in the detector and the vehicle by cosmic-ray protons. Obviously more direct methods for determining the energy spectrum of the neutrons should be made.

III. Requirements Imposed on the Space Neutron Monitor

To measure effectively the neutron flux above the atmosphere the neutron space monitor must have the following characteristics:

1. response to neutrons in the energy range of $.01 < E_n < 14 \times 10^6$ ev;*

---

*A recent review (Hess, 1963) on the possible sources for the radiation trapped in the inner radiation belt concludes that protons with energies greater than 5 Mev are due to albedo neutrons from both galactic and solar cosmic rays, and possibly a source for those electrons with energies less than 780 Kev. Even though these conclusions may be subject to debate, they do suggest some desirable properties for the monitor we are developing. Unfortunately, it was not feasible to require the monitor to have a significant response above E_n = 20 Mev. Thus, we would not be measuring directly those neutrons with $E_n > 30$ Mev which decay into energetic protons in the inner belt ($E_p > 30$ Mev). On the other hand, the neutron albedo spectrum produced by galactic cosmic rays is due to the slowing down and diffusion in the atmosphere of the evaporation neutrons ($\sim$4 Mev) and the knock-on neutron sources. Therefore, the lower energy neutrons are genetically related to the higher energy neutrons. We should also note that changes in the intensity of the galactic cosmic rays should be reflected in changes in the intensity of the albedo neutrons observed with the proposed monitor. On the other hand, we would expect albedo neutrons produced by solar protons to arise predominantly from an evaporation source because of the much steeper energy spectrum of the solar protons. The energy response of the proposed detector is therefore well suited for monitoring these neutrons.

2. significant efficiency over the above energy range, especially at high energies, with a minimum weight and volume;

3. negligible response to gamma rays and charged particles;

4. good voltage pulse-height distribution, with a clear separation of neutron and charged particle pulses;

5. minimum quantity of high atomic number material in the detector itself;

6. reliable and simple associated electronics;

7. shock resistant to approximately 50 g;

8. temperature stability of counting rate over the range from -30° to 70° C.

The types of detectors considered for incorporation in the space monitor were:

1. a BF_3 counter surrounded by 1/2 inch paraffin monitor;

2. a high pressure He^3 detector surrounded by approximately 1 inch of polyethylene;

3. a LiI (Eu) scintillator mounted on a photomultiplier surrounded by a 1 inch polyethylene moderator;

4. a Li^6 (ZnS) scintillator (Nuclear Enterprise Model 421), surrounded by a 1 inch polyethylene moderator.

The choice of the best neutron detector for incorporation in the neutron space monitor was based upon the following tests:

1. a careful evaluation of the pulse-height distribution of the neutron counter;

2. the discrimination in the detector against charged particles and gamma rays;

3. the efficiency over a range of energies from $.01 < E_n < 10 \times 10^6$ ev.

A moderated neutron detector selected on this basis was then incorporated with the charged particle counters to discriminate against production in the monitor. The effectiveness of the over-all detector was evaluated for rejection of charged particle events. A prototype unit of this system was designed and carefully tested.

IV. Comparison of Detector Characteristics

The comparison of the efficiencies of the BF_3 and He^3 gaseous counters and the Li^6I scintillation detector for neutrons depends upon the reaction cross-section. In Fig. 1 the reaction cross-section for He^3, B^{10}, and LiI, is shown as a function of neutron energy. The probability of interaction in a detector, assuming a directional flux perpendicular to the long axis of the counter is given by

$$\epsilon_t = S \left[1 - \exp\left(-L\left(\frac{p}{p_o}\right)\sigma_R t\right)\right] \text{ cm}^2 \qquad (1)$$

where p and p_o are the pressure in the detector and pressure at 0^o C, S is the cross-sectional area of the counter in cm^2, L is Loschmidt's number ($=2.6 \times 10^{19}$ cm^{-3} at STP). σ_R is the reaction cross section in cm^2, t equals the counter thickness in cm. From Fig. 1 it is evident that with equal numbers of atoms in these three possible detectors, the efficiency decreases rapidly with increasing neutron energy. Therefore, to extend the range of the detector to higher energy, it is necessary to surround it with a hydrogenous moderator to slow down the high energy neutrons. It is also interesting to note that the reaction cross-section for He^3 and B^{10} is almost a

monotonic function of energy, whereas for Li^6 there is a distinct resonance at approximately 500 Kev.

To compare these detectors we have studied their voltage pulse height distributions with a RCL 256-channel pulse height analyzer and the resulting pulse height distributions are shown in Figs. 2-5. The BF_3 proportional counter was 2" in active length, with 1" active diameter filled to a pressure of 60 cm. Hg., and was surrounded by a 1/2" paraffin moderator. This detector was chosen because it was similar to one previously flown in neutron experiments (Trainor and Lockwood, 1963). Two different He^3 detectors were used: one 4" in active length, with 1" diameter, filled to 10 atmospheres pressure and surrounded by a 1" polyethylene moderator. The second He^3 detector was 6" in active length, with 1" diameter, filled to 4 atmospheres of pressure and surrounded by a 1/2" polyethylene moderator. The LiI (Eu) scintillator was 1" in diameter, 4 mm thick, and was mounted on a 6199 photomultiplier, and encased in a 1" polyethylene moderator.

In the pulse height distribution curve for the gaseous BF_3 counter (Fig. 2), run with a source of thermal neutrons, it is quite evident that the noise and gamma ray pulses lie below 2 millivolts and that there is a broad distribution of pulses resulting from the neutron reaction products: alpha particles and Li recoil nuclei. The exposure of the detector to an intense flux

of gamma rays does not affect the integrated neutron counting rate provided that the discriminator level is set as indicated. The pulse height distributions for the He^3 proportional counters, shown in Figs. 3 and 4, were also obtained with a thermal neutron flux. The pulses from neutron reaction products producing the ionizing events are much greater than gamma-ray pulses, although the separation, or valley, between the noise and gamma pulses and the neutron events is not as sharp as with the BF_3 counter. However, with discrimination levels indicated in either Fig. 3 or Fig. 4, the contribution for the LiI scintillator shown in Fig. 5 was obtained for a thermal flux of neutrons. The pulse height distribution shown clearly indicates poor resolution of the neutron- and gamma-induced events. Therefore, some scheme must be used to reduce the response to gamma rays. Whether this can be done by pulse shaping techniques on the Li^6I scintillator is unknown at this time. Phoswiching techniques are quite reliable, but they do complicate the electronics for a detector. In discussing the efficiency of this detector, we must replace Loschmidt's number L, appearing in Eqn. 1, with $N_o \rho/A$, where N_o is Avagadro's number, ρ = the density of the scintillator material, and A = the atomic number. The details on the LiI neutron detector, including the phoswiching circuits are presented in Appendix B.

The pulse height distribution of a Li^6 (ZnS) Model NE 421 neutron scintillation detector was determined as shown in Fig. 6. This detector is similar to a LiI detector except that the Li^6 with 96% enrichment is dispersed in a zinc

sulphide matrix with silver as the activator. Relative to the LiI scintillator, the NE 421 is more efficient for neutrons because the cross-section of ZnS is higher for the capture of the nuclear reaction products. The ZnS, however, has poor light transmissivity, thus limiting the thickness of the scintillator. The neutron energy range and response are thus somewhat limited. The NE 421, however, has a very low gamma-ray response because the energy lost by the gamma rays is considerably less than in a Li^6I crystal. The pulse height distribution, as shown in Fig. 6, is very poor. The pulses from the neutrons and gamma rays can not be easily separated unless the discrimination level is set very carefully for counting. Since the differential pulse height distribution is a steep function of pulse height voltage, the stability required in the amplifier and discriminating circuit for a constant integrated neutron counting rate is much greater than for any of the detectors discussed so far. The poor pulse height distribution with low overall efficiency led us to reject this type of detector for the space monitor.

V. Discrimination Against Neutron Production in the Monitor

Neutrons will be produced in the detector and surrounding moderator by protons and neutrons with energies greater than about 50 Mev (Trainor, 1964). From the neutron albedo energy spectrum of Lingenfelter (1963) about 5% of the neutrons leaking from the atmosphere have energies greater than 3 Mev, of which only a small fraction of this energy will produce reactions. The intensity of protons,

however, with energies of greater than 1 Bev is about 20 times the intensity of neutrons with energies greater than 10 Mev. Hence, the larger source of production is from energetic protons through nuclear star reactions. The resulting cascade and evaporation neutrons will have a wide distribution in energy. Some of the fast cascade particles may induce secondary reactions with further production of evaporation neutrons. To discriminate against these production neutrons in the monitor, the neutron detector, or monitor, is surrounded by a charged particle detector. Whenever the detector responds to a charged particle, the resulting voltage pulse blanks off the neutron counting channel. This blanking time is set to be several life times of the neutrons in the moderator to eliminate practically all the neutrons produced by high energy particles.

There are several methods which may be used to surround the neutron counter with a charged particle detector system. Gaseous proportional counters can be placed either between the moderator and the neutron detector, or around the outside of the moderator. These proportional counters may be operated either in the additive mode or the coincidence mode. It is more desirable to have the charged particle detectors outside the moderator. In previous detectors used we placed the charged particle detectors inside the moderator. There are two bad features in such a scheme: (1) neutrons will be counted which are unaccompanied by charged particles, these events occurring as a result of high energy protons incident on the moderator. (2) The

threshold for charged particle detection is quite high, about 40 to 80 Mev, because the charged particles must penetrate through the moderator. The arrangement with the charged particle counters outside the moderator is much better, but does require a large number of charged particle detectors, with the possibility, therefore, of having the counting system saturate. In another scheme to detect the charged particles, a moderator which is also a scintillator is used. With the photomultiplier located at one end of the detector, the system may be adjusted to reject charged particle events through a gating signal. This method is much more complicated than the charged particle counter system, but is quite feasible.

With the Li^6I scintillator generally a hydrogenous scintillator is used as a moderator to surround the neutron detector. Then standard pulse shaping techniques can be employed. One type is described in detail in Appendix B. The results of a similar system for fast neutron detection will be discussed in Section X. For examples of such detectors, see Haymes (1964) and Mendell and Korff (1963).

VI. Comparison of the Efficiencies of the Neutron Monitors

The neutron space monitors were calibrated by exposing them to known neutron fluxes in the energy range $.01 < E_n < 14 \times 10^0$ ev. The 400 Kev Van de Graaff accelerator at the University of New Hampshire provided a source of nearly monoenergetic neutrons at 14, 5, 3, and 0.1 Mev by using tritium, copper, deuterium, and carbon targets. The absolute flux was determined by irradiating foils and comparing the counting rates of a standard long counter (Hanson and McKibben, 1947; and Marion and Fowler, 1960). In addition, calibrated Ra-Be and Pu-Be sources were used to provide

neutrons with mean energies of 4.1 Mev and 3.5 Mev, respectively. Thermal energy calibrations were made at the thermal neutron facilities of the Portsmouth Naval Shipyard and with the target of the Van de Graaff accelerator surrounded by a large paraffin moderator. The principle difficulty in calibrating monitors for fast neutrons with the Van de Graaff accelerator arises from the back scattering of neutrons from the walls surrounding the target. These neutrons will have much lower energies, and since all detectors being considered have an efficiency inversely dependent upon energy, the scattering effect may mask the response to fast neutrons. The experimental set-up used for calibrating the monitors is shown in Fig. 7 with the Van de Graaff operated to produce a continuous flux or pulsed beam of neutrons.

In earlier attempts to calibrate the neutron monitors, the Van de Graaff had been pulsed and both the long counter and neutron monitor pulsed in synchronization with the accelerator pulse. This method reduces the effect of scattering since the time between pulses was the order of milliseconds, and in this time the neutron flux in the room would decay to essentially zero. However, a large correction must be made for the finite rise and decay of the neutron gas in the moderator of the monitor and the long counter used for calibration, and any small leakage of deuterons down the accelerating column of the Van de Graaff in between pulses would produce large errors in the measured efficiencies. The leakage problem was a major one because the Van de Graaff could not be made to operate properly at the necessary low

beam currents. Since the correction for the finite rise and decay of the neutrons in the moderator was very large, it was decided to discard this method.

To reduce the scattering of neutrons by the walls of the room, the fast neutron beam was collimated by means of paraffin and the energy degraded neutron flux was then partially absorbed by cadmium and boral plate (Fig. 8). A check can be made on the scattered intensity by the $1/R^2$ response with detectors or foils which respond to the fast flux only and to the total flux. It was found that with the collimated beam the response was nearly $1/R^2$ in the region where the monitor was located for calibration purposes. The arrangement of the collimator is shown in Fig. 8 and effect upon the neutron is plotted in Fig. 9, where the relative response is plotted against the angle α, with the geometrical shadow of the collimator indicated by the vertical dashed line. This response enabled us to correct for the background of the scattered neutrons at the monitor. The efficiency can then be redefined by

$$\epsilon = \frac{R_m\ (0^\circ) - R_m\ (15^\circ)}{\phi_f} \qquad (2)$$

As mentioned previously, we can determine the fast flux from the induced activity in various foils having the appropriate neutron energy thresholds. A detailed discussion of such methods can be found in Allen (1960) and Marion and Fowler (1960).

The most reliable method for calibrating the Van de Graaff neutron flux is to count the associated particles.

This technique enables one to determine the flux to approximately ± 5 percent. This method is most reliable with the tritium target since the associated recoil alpha particle has an energy of about 3 Mev. The neutron flux calibration by this method agreed to within 15 percent of the results using the induced activity of foils. The experimental set-up for the associated particle assembly is shown in Fig. 10.

To calibrate with Ra-Be and Pu-Be sources it must be noted that these are not monoenergetic sources of neutrons and the known energy spectra (Fowler, 1960) must be folded into the estimated efficiency of the detector. If the response of the monitor is given by S(E) counts/neutron/cm^2, and the number of neutrons emitted from the source with a given energy E is defined as N(E), then the mean energy for the source as seen by the monitor will be given by

$$\bar{E} = \frac{\int E\ N(E)\ S(E)dE}{\int N(E)\quad (E)dE}$$

The integral can be replaced by a summation, in which N(E) and S(E) are considered essentially constant over small energy intervals. Consequently, a radioactive source can only be used as a check on the absolute calibration of the monitor, since the relative response of the monitor must be known approximately to calculate the mean energy of this source. However, the efficiency of the neutron monitor can be determined approximately by considering the measured efficiency to correspond to the actual mean energy of the neutrons from the radioactive source.

In addition, the neutron detectors were calibrated in an intense flux of low energy gamma rays and the results of these calibrations are summarized in Table II.

It can be seen from Table II that the He^3 neutron monitor has the highest neutron efficiency. Its efficiency is larger than the LiI scintillator. While the latter is a somewhat smaller detector, the high gamma response of the scintillator suggests that it would not be as good for space measurements. The BF_3 monitor, with the lowest gamma-ray response, has an almost correspondingly lower neutron efficiency. Increasing the size of the BF_3 detector would increase its efficiency, but unless the gas pressure in the counter were greater than an atmosphere, it could not compare with the He^3 detector. A very distinct advantage of the He^3 detector is its very low operating voltage for correspondingly high efficiencies. The pulse height voltage distribution of the He^3 neutron detector is good enough for circuits used. We found that the He^3 detector had a negligible temperature coefficient from about -30° C to $+50^\circ$ C. Therefore, the only temperature stability problem for this type of detector is in the temperature compensation of the electronics, which is easily achieved. The He^3 monitor also seems the best choice in view of size and weight considerations. Scintillator-type monitors must be considerably larger because at least one or two photomultipliers are required. The only major disadvantage of the He^3 monitor is its lack of a 4π solid angle to detect charged particles for discrimination against local production of neutrons.

Table II. Efficiencies $[S(E_n)]$ of Monitors (cts/n/cm^2)

Method of Calibration	4" He^3 1" Mod.	6" He^3 1/2 Mod.	Li^6I 1" Mod.	NE421 1" Mod.	2"$B^{10}F_3$ 1/2 Mod.	He^3 Prototype	Trainor's CRM7B
I. Van de Graaff Accelerator:							
1) Pulsed Mode:							
Energy:							
14.2 Mev	3.20	2.08	0.58	-	0.098	-	0.118
5.0 Mev	3.80	2.46	0.28	-	0.043	-	0.151
3.2 Mev	3.10	2.01	1.32	-	0.109	-	0.169
119 Kev	9.45	6.15	1.95	-	0.161	-	0.425
2) Collimated Beam:							
Energy:							
14.2 Mev	3.94	4.05	2.51	0.323	0.146	-	-
5.0 Mev	4.84	4.43	2.32	-	0.164	-	-
3.2 Mev	4.84	4.45	2.91	-	0.174	-	-
119 Kev	6.66	5.55	-	-	0.206	-	-
3) Paraffin Added to Collimator:							
Energy:							
14.2 Mev	2.04	1.98	1.67	-	-	1.73	-
5.0 Mev	2.30	2.06	1.45	-	-	1.95	-
3.2 Mev	2.58	2.31	1.83	-	-	2.19	-
119 Kev	3.46	2.60	-	-	-	2.94	-
4) Thermal Energy:	21.70	19.62	9.30		1.47	21.7	

Table II. Efficiencies $[\bar{S}(E_n)]$ of Monitors (cts/n/cm^2) (Continued)

	Method of Calibration	4" He^3 1" Mod.	6" He^3 1/2 Mod.	Li^6I 1" Mod.	NE421 1" Mod.	2" $B^{10}F_3$ 1/2 Mod.	He^3 Prototype	Trainor's CRM7B
II.	Sources:							
	1) Ra-α-Be:							
	Mean Energy = 4.11 Mev	2.38	1.71	1.56	-	-	1.95	0.151
	2) Pu^{239}-α-Be:							
	Mean Energy = 3.46 Mev	2.48	1.79	-	-	-	2.06	-
	3) Thermal (PNSF):	18.21	18.23	-	-	1.20	18.21	1.090
	4) Co^{60}:							
	(cts/γ/cm^2) (x10^{-5})	1.37	2.84	54.0	1	.769	1.37	1
III.	$\bar{S}$							
	(cts/n/cm^2)	-	-	-	-	-	5.88	0.33

However, the fraction of solid angle in which charged particles may enter without being detected is about 5 percent of the total solid angle. Consequently, this is not a serious disadvantage, and can be neglected in an isotropic flux of particles. In conclusion, therefore, these tests indicate that He^3 neutron monitor is the best choice for a space neutron monitor in terms of the requirements proposed at the outset of this study.

VII. Design of a Prototype Monitor

On the basis of these conclusions we have designed a prototype, the tube module for which is shown in Fig. 11. On the center is located the He^3 counter, 4" active length and 1" active diameter, filled to a pressure of 10 atm. Although the design with the charged particle proportional counters on the outside of the monitor is more desirable, the proportional counters were located as shown in Fig. 11, because we did not have available sufficient proportional counters for the outside with a moderator of the proper geometrical shape. The polyethylene moderator was approximately 1/2" in diameter, which is less than the optimum diameter of 1", which reduced the efficiency about 20%, as indicated in Table II. The tube module is separate from the electronics and is capable of being operated at distances of several feet from the main electronics module. The schematic diagram of the electronics is indicated in Fig. 12, and detailed circuit diagrams are presented in Appendix A.

In Figs. 13 and 14 are shown two views of the detector and the associated electronics. The calibration curve for the prototype is shown in Fig. 15. Since the He^3 neutron monitor has cylindrical geometry, the efficiency as a function of angle has been determined using the scheme indicated in Fig. 16, and the results of this calibration are shown in Fig. 17. We see that the efficiency drops by a factor of approximately 2.50 in a direction along the axis of the counter where there is no monitor. The region between thermal energies and 10^6 electron volts was sketched in, using the known response of a neutron detector with approximately 1" polyethylene. This curve will be treated in more detail when more satisfactory neutron fluxes ($E_n \sim$ 100 Kev) have been obtained from carbon targets. In Table III are listed the specifications for the prototype space neutron monitor. The mean efficiency for the prototype unit for the Lingenfelter neutron flux (1963) is 5.88 ± 1.18 cts/neutron/cm^2.

VIII. Directional Neutron Detectors for Space Measurements

Preliminary investigations have been made of a type of directional neutron detector for neutron measurements in space, particularly solar neutrons. The results of the first series of experiments with this detector have been presented in Progress Report No. 1 (NASr-211, Dr. E. L. Chupp, Principal Investigator), and only a brief summary of results here. Extensive investigations are being conducted by Dr. Chupp to increase the size and efficiency to obtain sufficiently high counting rates.

Table III. Specifications for Space Neutron Monitor Prototype

Dimensions:

1) Tube Module - 3.5 in. diameter; 10.5 in. long

2) Electronics Module - 10.5 x 2.5 x 5.5 inches

Counters:

1) He^3 tube - high voltage = 1575 V; disc. = 1 mv.

2) Prop. Bank A - high voltage = 2050 V; disc. = 3 mv.

3) Prop. Bank B - high voltage = 2050 V; disc. = 3 mv.

Energy Range:

1) Neutrons = $0.01 < E_n < 14 \times 10^6$ ev

2) Protons = approx. > 40 Mev and > 80 Mev

3) Electrons = approx. > 1 Mev

Background: 0.6 cts/min in paraffin pile with Cd around tube module

Power: 1.5 watts

Weight: 10 lbs

Temperature Test:

(-30° C to 70° C) 1) Amplifier gain constant 5%

2) High voltage constant 0.5%

Shock Test: 10 g's sine wave

To consider the effectiveness of this type of directional detector two small prototypes similar to the design of Stetson and Berko (1959) were obtained from Nuclear Enterprise. These scintillators were in the form of right circular cylinders with a diameter of 3.8 cm. and a height of 2 cm. The one scintillator, designated as the "rod" scintillator, consisted of 97 plastic scintillating rods held in a parallel array by a non-scintillating plastic matrix. The other scintillator, designated as the slab type, consisted of 15 slabs also held in a parallel array by non-scintillating plastic. In Table IV are indicated the dimensions of the two detectors.

Table IV. Dimensions of Directional Neutron Detectors Tested

Type	Rod	Slab
d (cm)	10^{-1}	5×10^{-3}
S (cm)	3×10^{-1}	4×10^{-1}
A (cm^2)	0.75	1.7×10^{-2}

d = diameter of rods or thickness of slabs.

S = distance to nearest rod or slab.

A = total cross-sectional area of detector.

The results of tests with this type of directional detector are summarized in Table V. These measurements were made with 14 and 3 Mev neutrons produced in the Van de Graaff accelerator. It is clear that for neutrons of 14 Mev both the rod and scintillator detectors are highly directional. For 3 Mev neutrons, however, only the slab detector has a significant directional response. In all

Table V. Results of Tests on the Directional Detector

A. E_n = 14 Mev

	Rod				Slab			
Fraction Maximum Pulse Height	53	60	67	73 percent	53	63	68	74 percent
Half-width	160	70	60	50	65	55	50	45
Ratio Counting Rate at 0° to 90°	2.2	5.5	25	100	13	16	16	20
Efficiency (Percent)	1.2	0.9	0.6	0.4	0.6	0.4	0.3	0.2

B. E_n = 3 Mev

Fraction Maximum Pulse Height	53	62	72		53	62	75
Half-width	No directional effect				--	160	70
Basic Counting Rate at 0° to 90°	--	--	--	--	1	2.2	7.5
Efficiency (Percent)	2.8	1.1	0.6		1.5	0.9	0.5

cases when the counting rate is plotted against the angle θ between the axis of the rod and incident neutron beam, a distribution is obtained which is almost Gaussian, the maximum occurring at $\theta = 0$ and the minimum at $\theta = 90^{\circ}$. The half-width and the ratio of the counting rate at 0° to the counting rate at 90° depend directly upon the pulse discriminating level. It would seem that with the discrimination level at two-thirds the maximum pulse height the ratio of the counting rate for 14 Mev neutrons at 0° to that at 90° for both types of material is quite appreciable.

These preliminary results indicate the feasibility of trying to make a much larger detector with slightly different physical dimensions, a program to be carried out by Dr. E. L. Chupp. One feature to be considered in such a detector is the rejection of charged particle interactions. The cosmic-ray flux, consisting primarily of protons, will produce recoiling events. Therefore, this detector must be surrounded by a thin plastic in which the charged particles will generate an anticoincidence gating signal to bias off the neutron detector.

IX. Fast Neutron Detector

We have constructed a fast neutron detector using a stilbene scintillator with the pulse shape discrimination circuit of Daehnick and Sherr (1961). Preliminary tests have been made on the detector to determine the rejection ratio for gamma rays and the energy resolution for neutrons. No attempt has been made yet to encase the stilbene detector

in a thin plastic scintillator for discrimination against charged particle production.

Typical pulse height distributions are shown in Figs. 18a and 18b. The dashed curve in Fig. 18a (X 30 scale) is the pulse height distribution without p.s.d. for neutrons from the DD reaction with 400 Kev deuterons with an intense source ($\sim$1 mc, Co^{60}) of gamma rays present. The solid curve is the pulse height distribution for the neutrons only. The pulse shape discriminated output under the same conditions is shown in Fig. 18b. It is evident that the gamma pulse rejection ratio is very good, the measurements indicating that it exceeds 300/1. By the method of Broek and Anderson (1960) we can then deduce the neutron energy spectrum from the pulse height distribution shown in Fig. 18b.

Having acquired some experience with pulse shaping circuits and the methods used to derive a neutron energy spectrum from the proton recoil spectrum, we plan to investigate other types of recoil detectors for possible use to measure the neutron energy spectrum near the earth. Any such detecting scheme must, of course, incorporate an anticoincidence arrangement for charged particle rejection.

References

Albert, R. D., C. Gilbert and W. N. Hess (Abstract) J. Geophys. Research 67, 3537, 1962.

Allen, W. D., "Neutron Detection," Philosophical Library, Inc., New York 16, N. Y., 1960.

Bame, S. J. et al., Bull. Am. Phys. Soc. 5, 360, 1960.

Bame, S. J., J. P. Conner, F. B. Brumley, R. L. Hostetter, and A. C. Green, J. Geophys. Research 68, 1221, 1963.

Daehnick, W., and R. Scherr, Rev. Sci. Instr. 32, 666, 1961.

Haymes, R. C., J. Geophys. Research 69, 841, 1964.

Hess, W. N., E. Canfield, and R. E. Lingenfelter, J. Geophys. Research 66, 667, 1961.

Hess, W. N., H. W. Patterson, R. Wallace, and E. L. Chupp, Phys. Rev. 116, 445, 1959.

Hess, W. N., and A. J. Starnes, Phys. Rev. Letters 5, 48, 1960.

Lingenfelter, R. E., J. Geophys. Research 68, 5633, 1963.

Lord, J. J., Phys. Rev. 81, 901, 1951.

Marion, J. B., and J. L. Fowler, "Fast Neutron Physics", Techniques, Part I, Interscience Publishers, Inc. New York, 1960.

Mendell, R. B., and J. A. Korff, J. Geophys. Research 68, 5487, 1963.

Newkirk, L. L., J. Geophys. Research 68, 1825, 1963.

Peterson, L. E., and J. H. Nitardy, Rev. Sci. Instru. 32, 1390, 1961.

Rao, M. V. K., Science 141 (9 August 1963), 530.

Simpson, J. A., Phys. Rev. 83, 1175, 1951.

Stetson, R. F., and S. Berko, Nuclear Instr. and Methods 6, 94, 1959.

Trainor, J. H., and J. A. Lockwood, Trans. Am. Geophys. Union 44, 73 (1963) and private communication.

Williams, D. J., and G. O. Bostrom, J. Geophys. Research 69, 377, 1964.

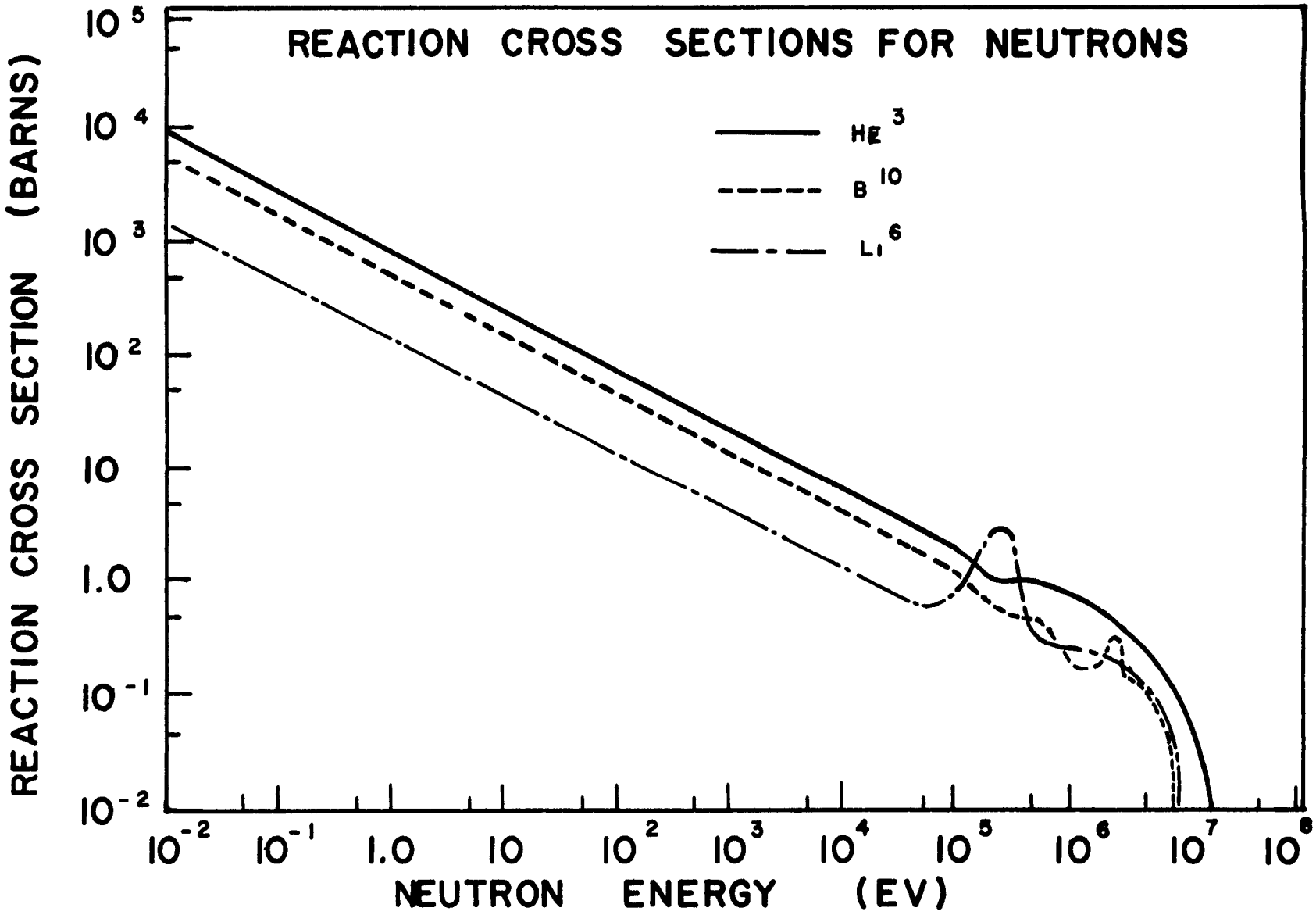
REACTION CROSS SECTIONS FOR NEUTRONS
REACTION CROSS SECTION (BARNS)
NEUTRON ENERGY (EV)
HE 3
B 10
LI 6
10 5
10 4
10 3
10 2
10
1.0
10 -1
10 -2
10 -2
10 -1
1.0
10
10 2
10 3
10 4
10 5
10 6
10 7
10 8

FIG. 1

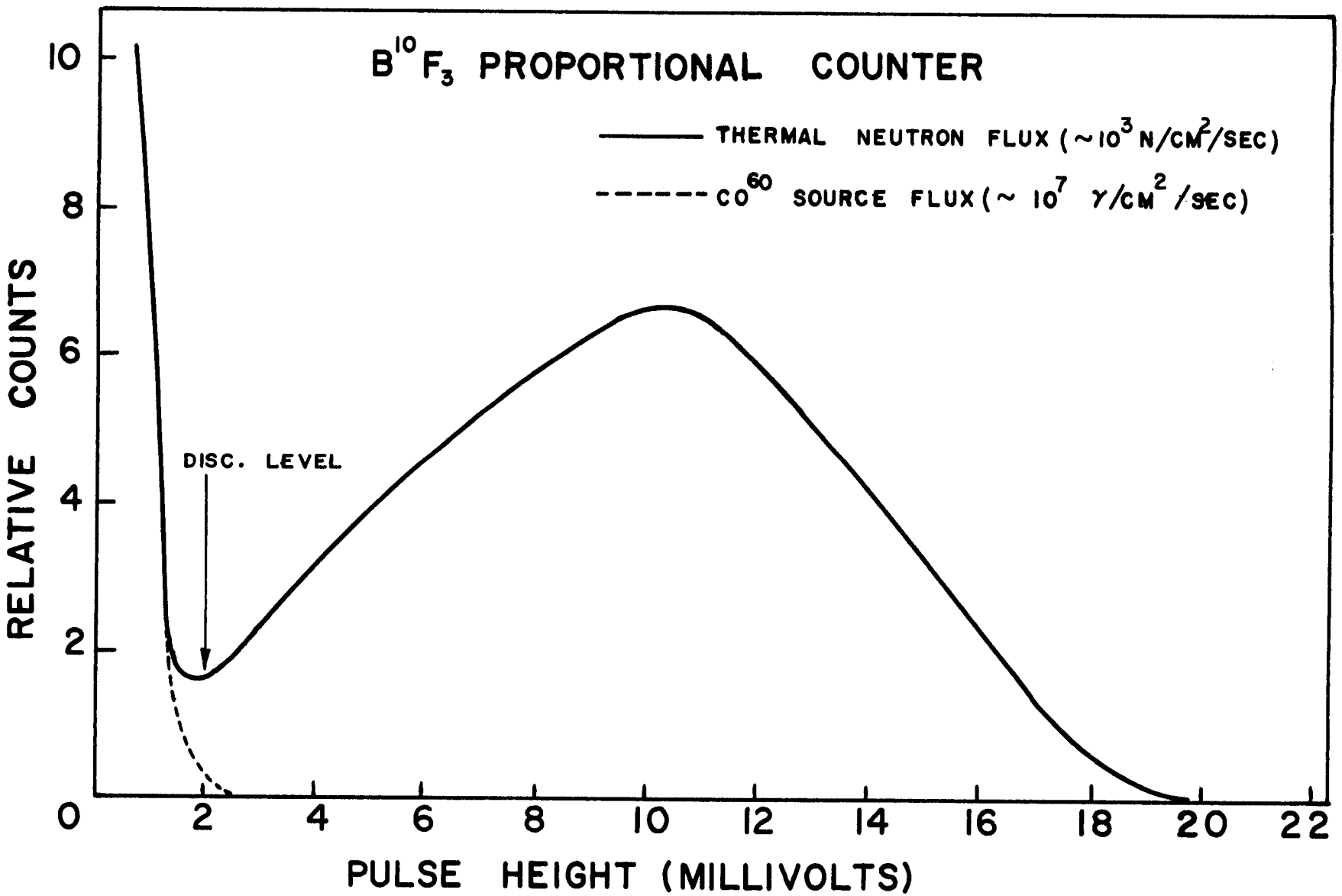
$B^{10}F_3$ PROPORTIONAL COUNTER
THERMAL NEUTRON FLUX ($\sim 10^3$ N/CM^2/SEC)
CO^{60} SOURCE FLUX ($\sim 10^7$ γ/CM^2/SEC)
DISC. LEVEL
RELATIVE COUNTS
0
2
4
6
8
10
2
4
6
8
10
12
14
16
18
20
22
PULSE HEIGHT (MILLIVOLTS)

FIG. 2

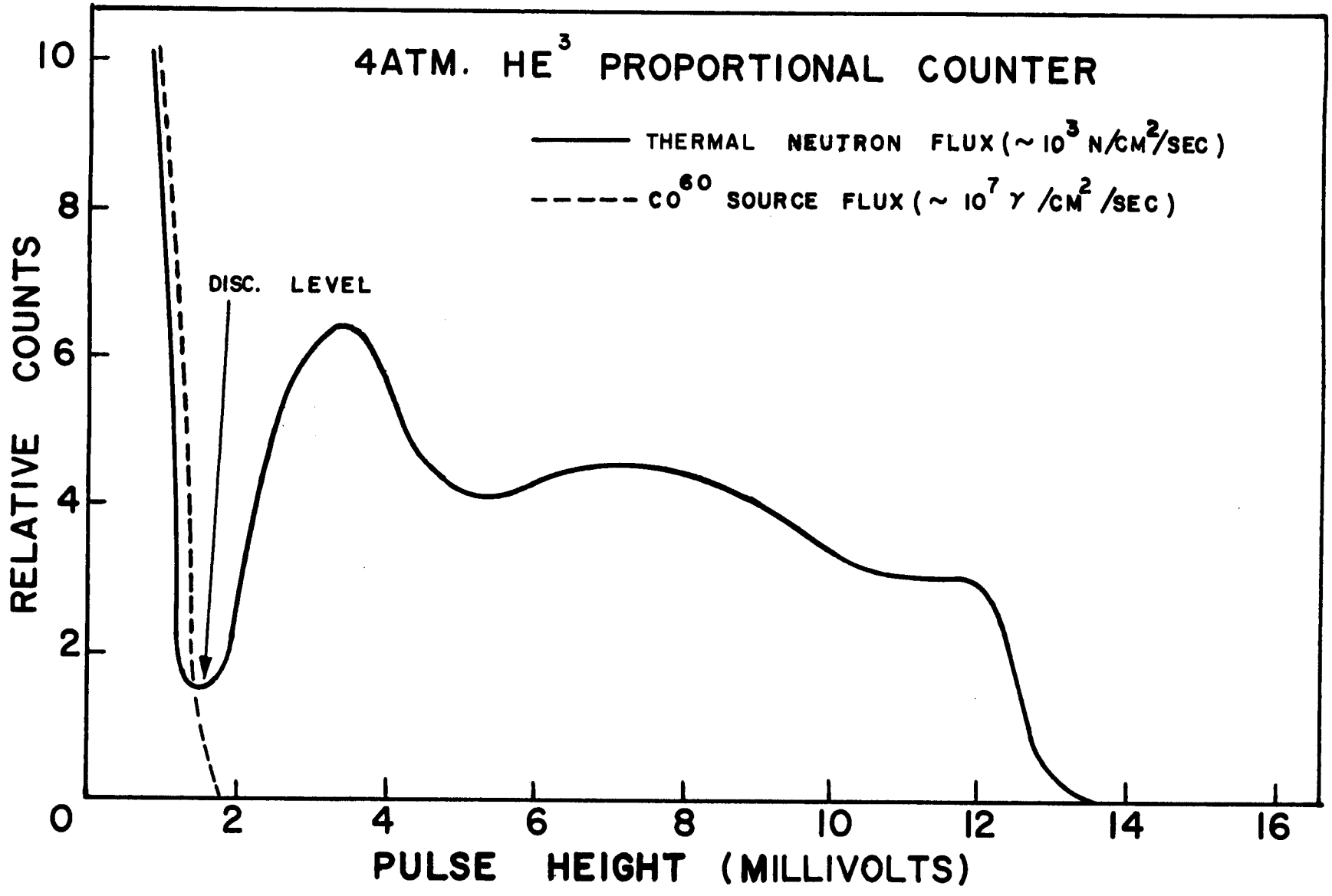
4ATM. HE3 PROPORTIONAL COUNTER
THERMAL NEUTRON FLUX (~ 10^3 N/CM^2/SEC)
CO^60 SOURCE FLUX (~ 10^7 γ /CM^2 /SEC)
DISC. LEVEL
RELATIVE COUNTS
0
2
4
6
8
10
PULSE HEIGHT (MILLIVOLTS)
2
4
6
8
10
12
14
16

FIG. 3

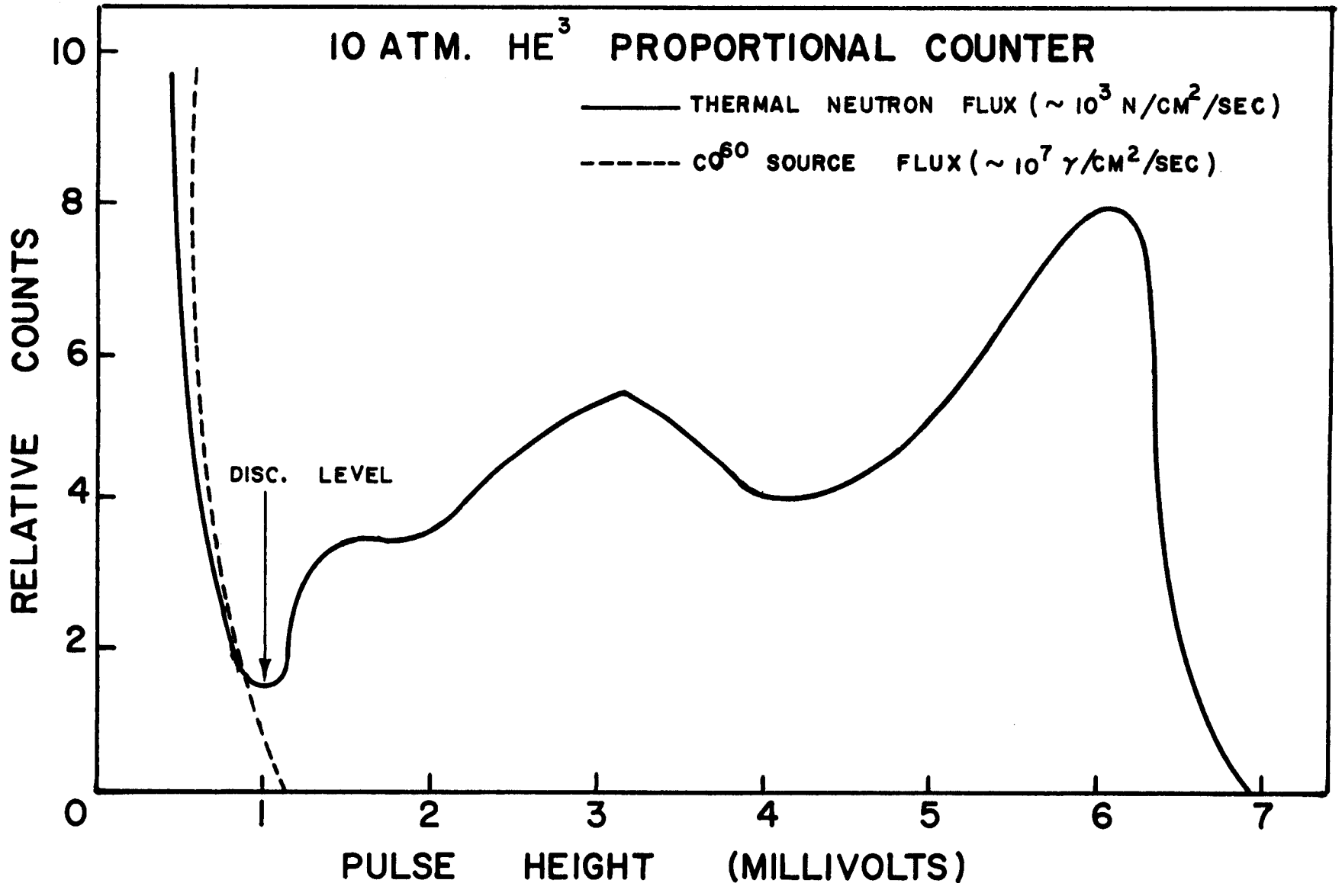
10 ATM. HE3 PROPORTIONAL COUNTER
THERMAL NEUTRON FLUX (~ 10^3 N/CM^2/SEC)
Co60 SOURCE FLUX (~ 10^7 γ/CM^2/SEC)
RELATIVE COUNTS
DISC. LEVEL
0
2
4
6
8
10
1
2
3
4
5
6
7
PULSE HEIGHT (MILLIVOLTS)

FIG. 4

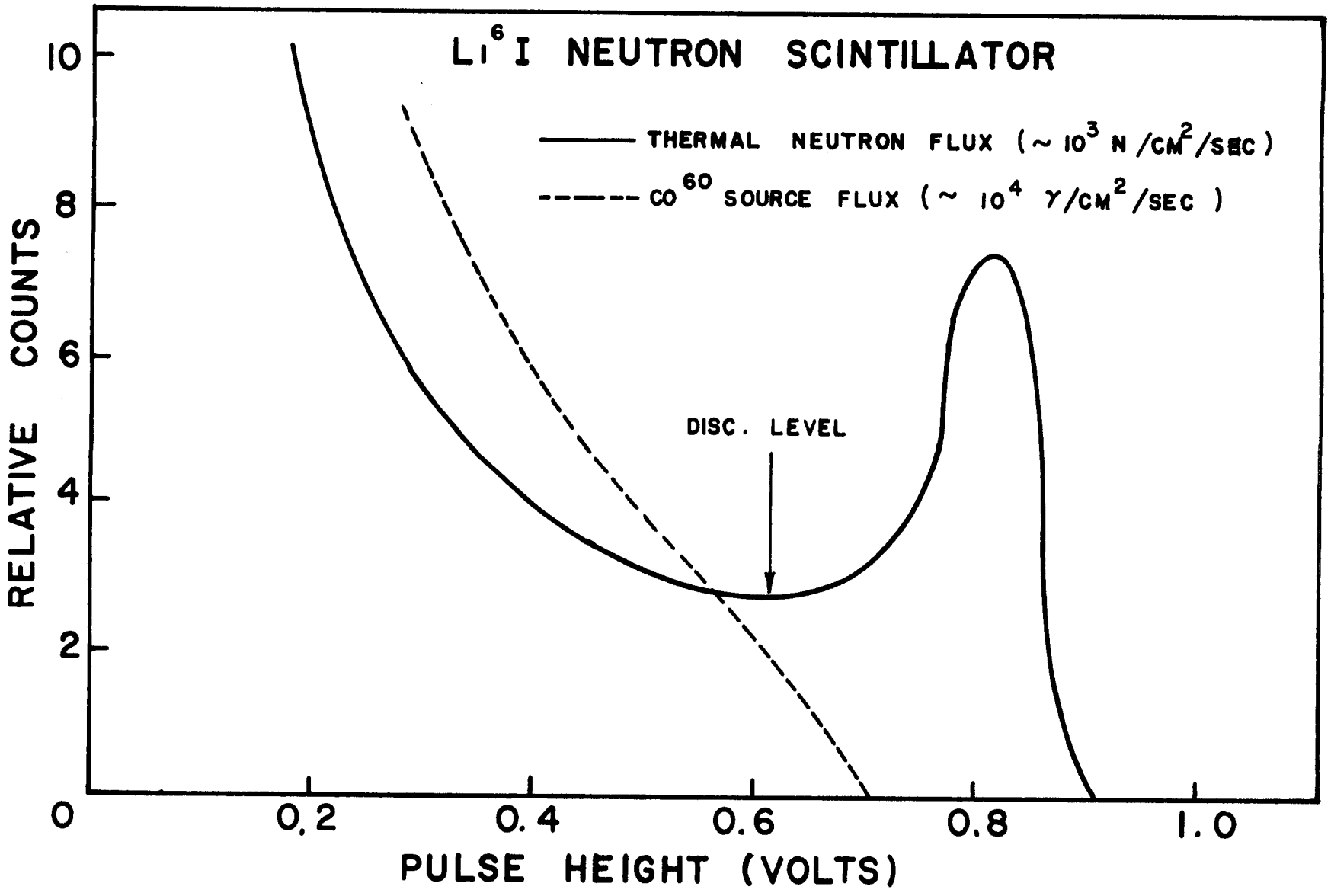
Li⁶I NEUTRON SCINTILLATOR
THERMAL NEUTRON FLUX (~ 10³ N/CM²/SEC)
Co⁶⁰ SOURCE FLUX (~ 10⁴ γ/CM²/SEC)
DISC. LEVEL
RELATIVE COUNTS
PULSE HEIGHT (VOLTS)
0
2
4
6
8
10
0.2
0.4
0.6
0.8
1.0

FIG. 5

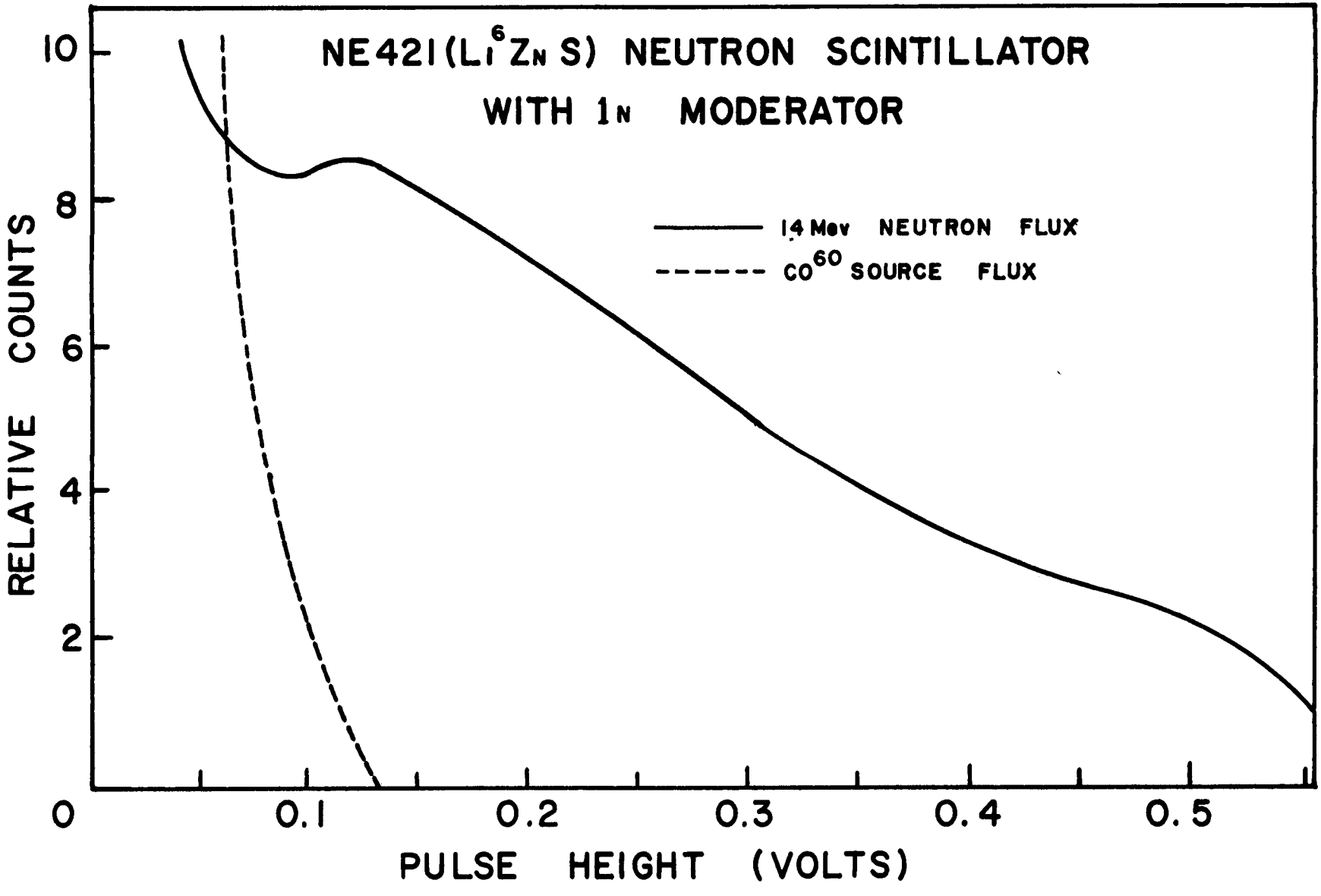
NE421 (Li^6 Zn S) NEUTRON SCINTILLATOR
WITH 1N MODERATOR
14 Mev NEUTRON FLUX
Co^{60} SOURCE FLUX
RELATIVE COUNTS
10
8
6
4
2
0
0.1
0.2
0.3
0.4
0.5
PULSE HEIGHT (VOLTS)

FIG. 6

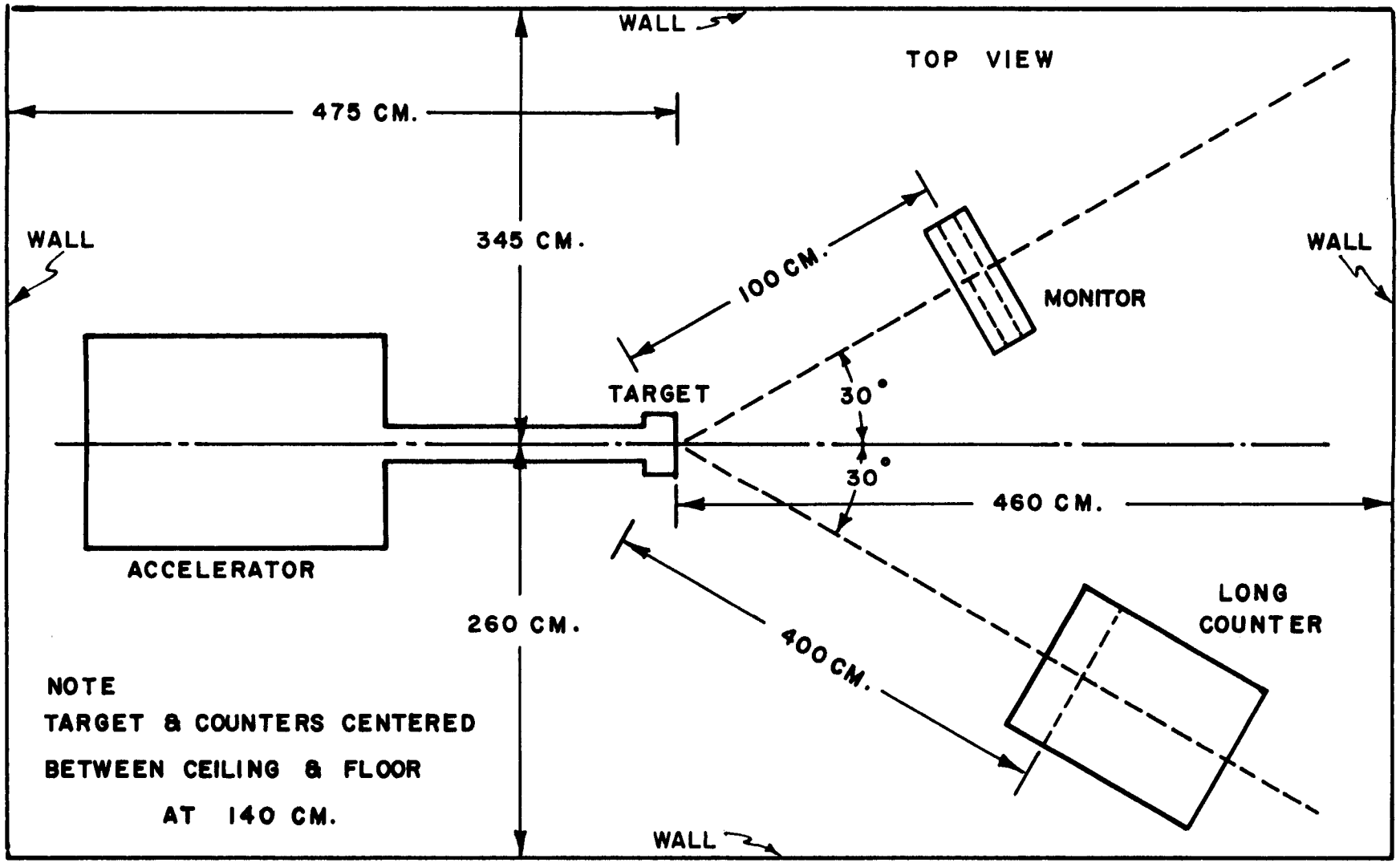

SET UP FOR D.C. & PULSED CALIBRATIONS

FIG. 7

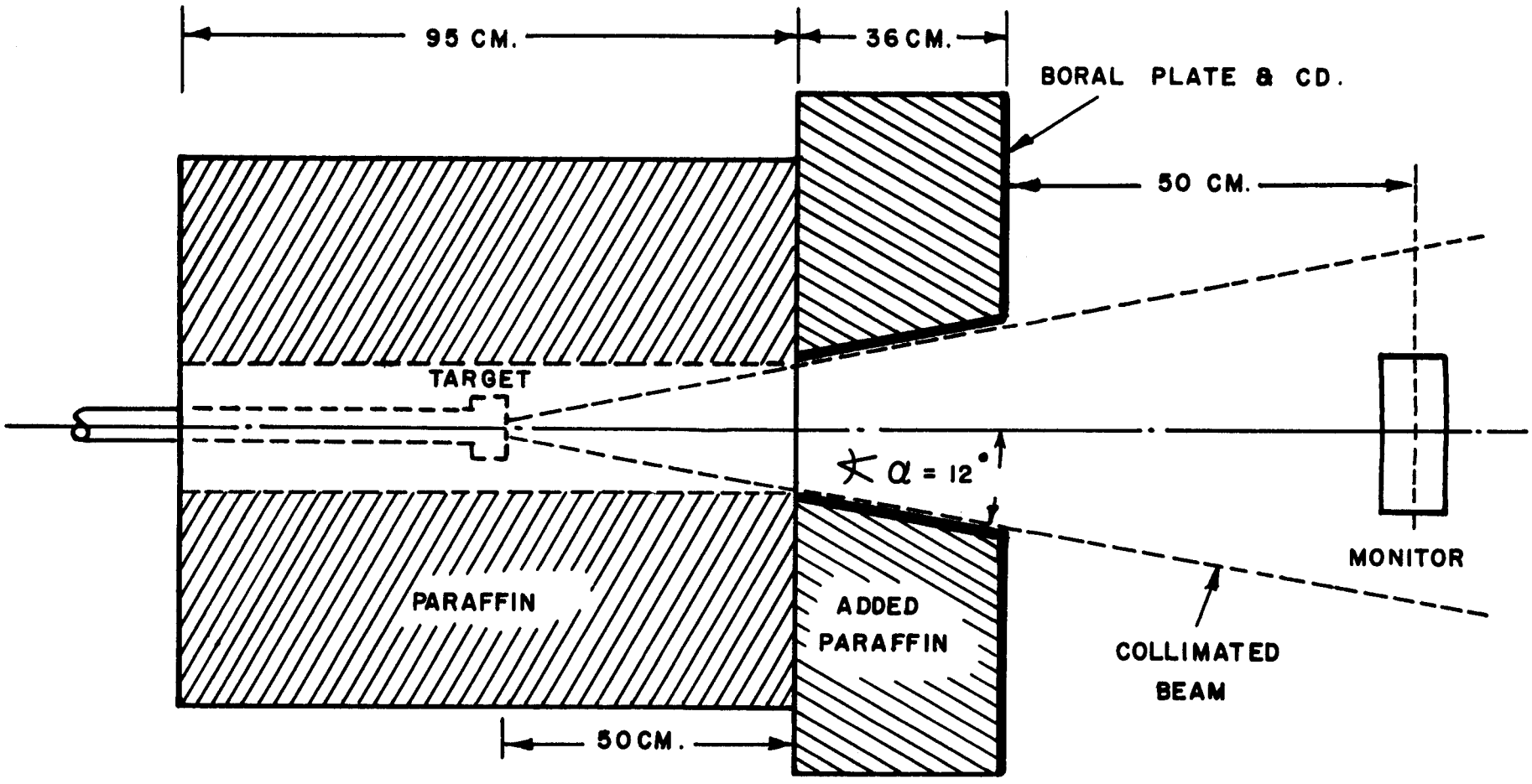

COLLIMATED BEAM SET UP

FIG. 8

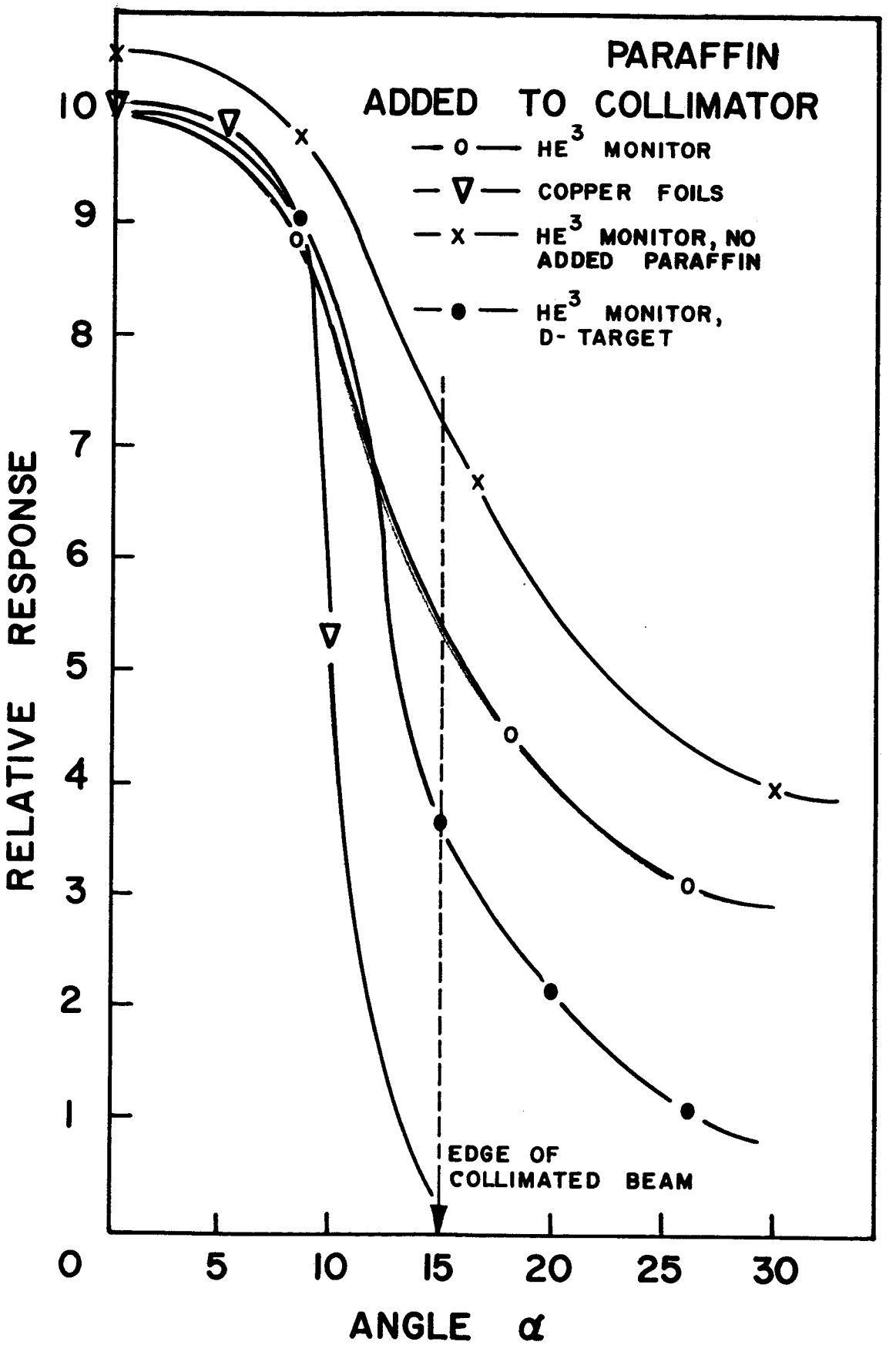
PARAFFIN
ADDED TO COLLIMATOR
— o — HE3 MONITOR
— ∇ — COPPER FOILS
— x — HE3 MONITOR, NO ADDED PARAFFIN
— ● — HE3 MONITOR, D- TARGET
RELATIVE RESPONSE
ANGLE α
EDGE OF COLLIMATED BEAM
0
1
2
3
4
5
6
7
8
9
10
5
10
15
20
25
30

FIG. 9

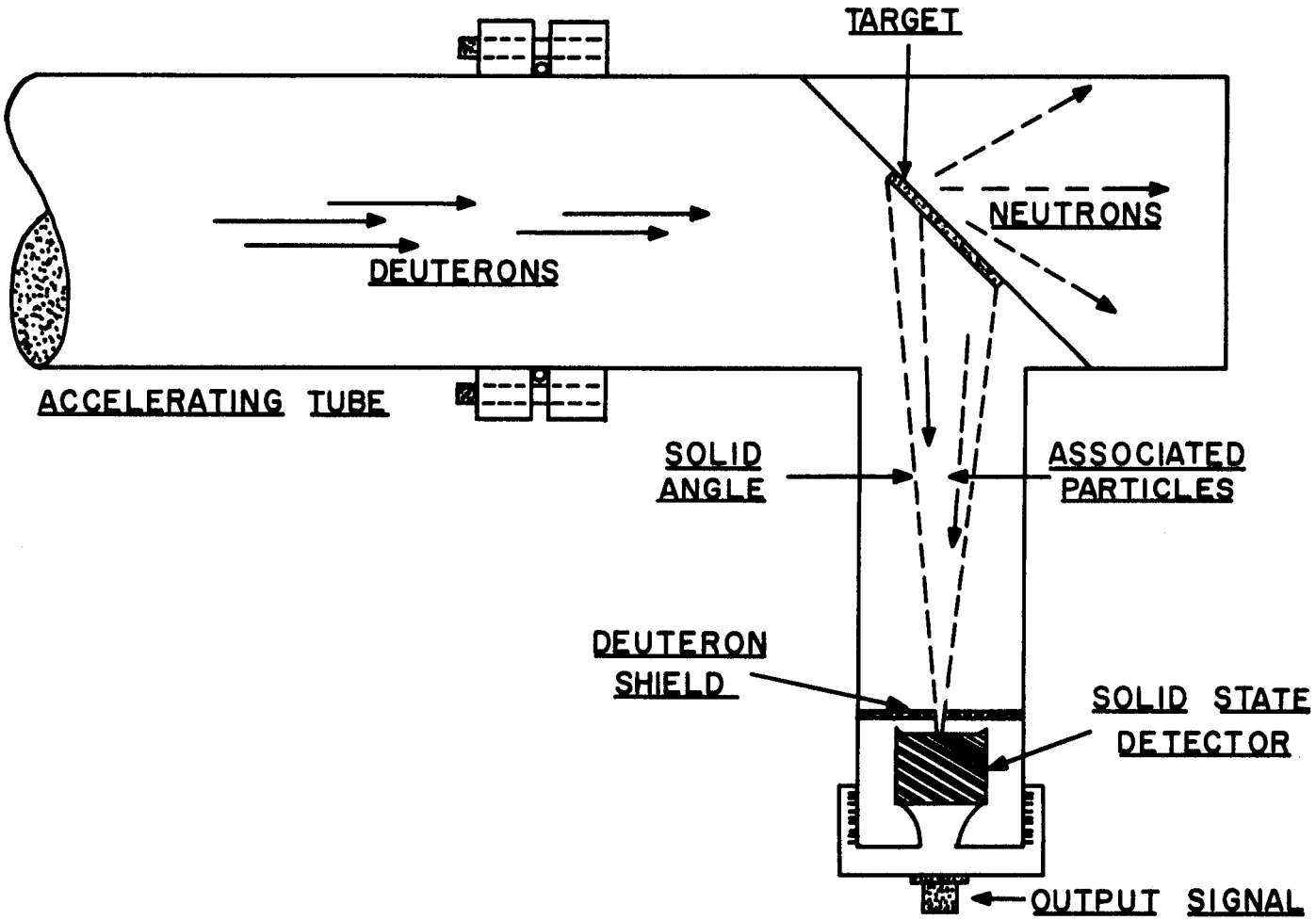

ASSOCIATED PARTICLE ASSEMBLY

FIG. 10

PROTOTYPE TUBE MODULE

END VIEW

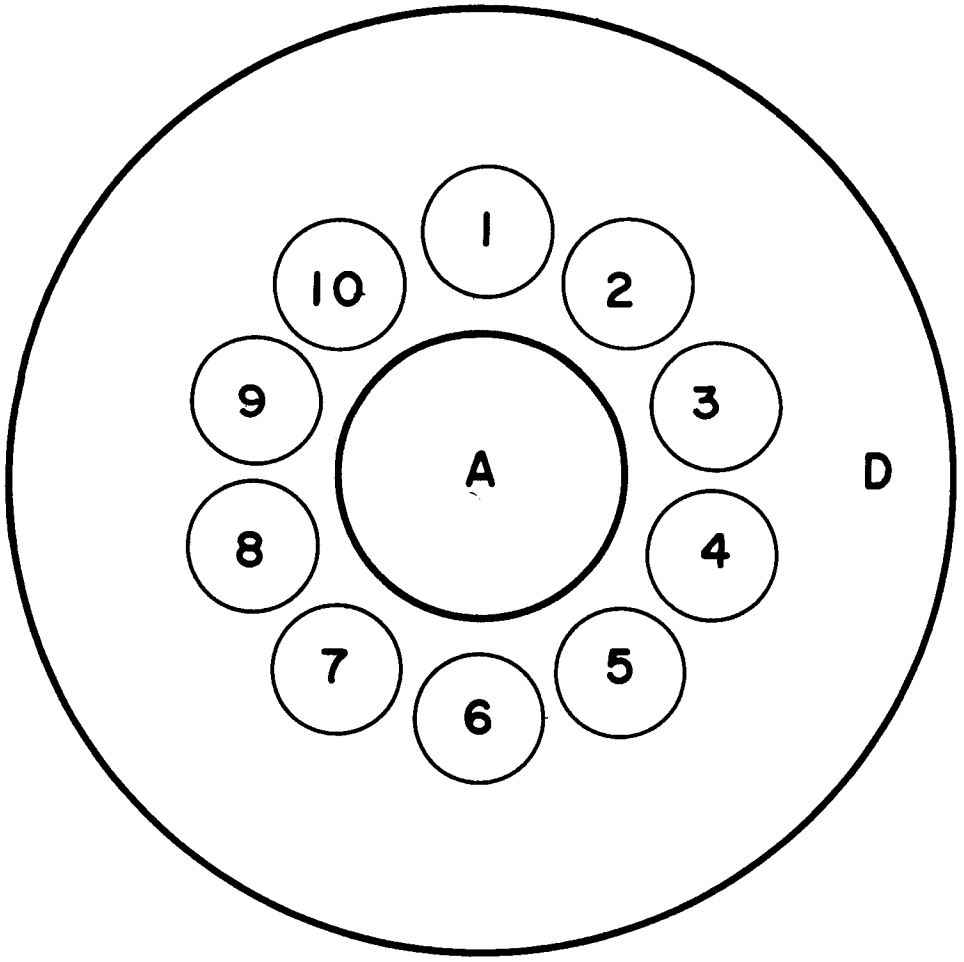

TUBE ARRANGEMENT

(1-5) BANK A – PROPORTIONAL COUNTERS

(6-10) BANK B – PROPORTIONAL COUNTERS

(A) HE^3 NEUTRON COUNTER

(D) POLYETHYLENE MODERATOR

FIG. 11

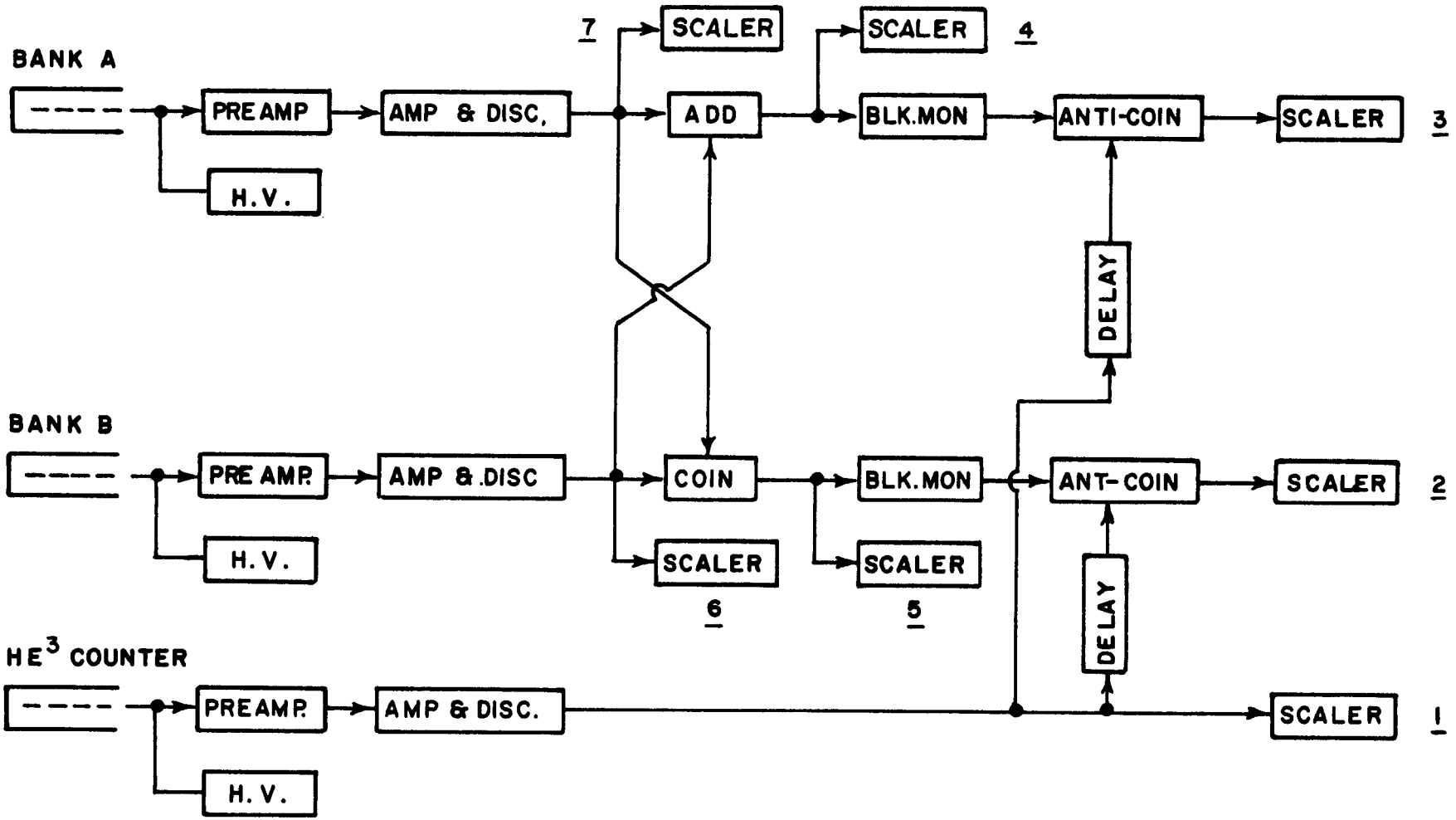

BLOCK DIAGRAM FOR PROTOTYPE

FIG. 12

OUT

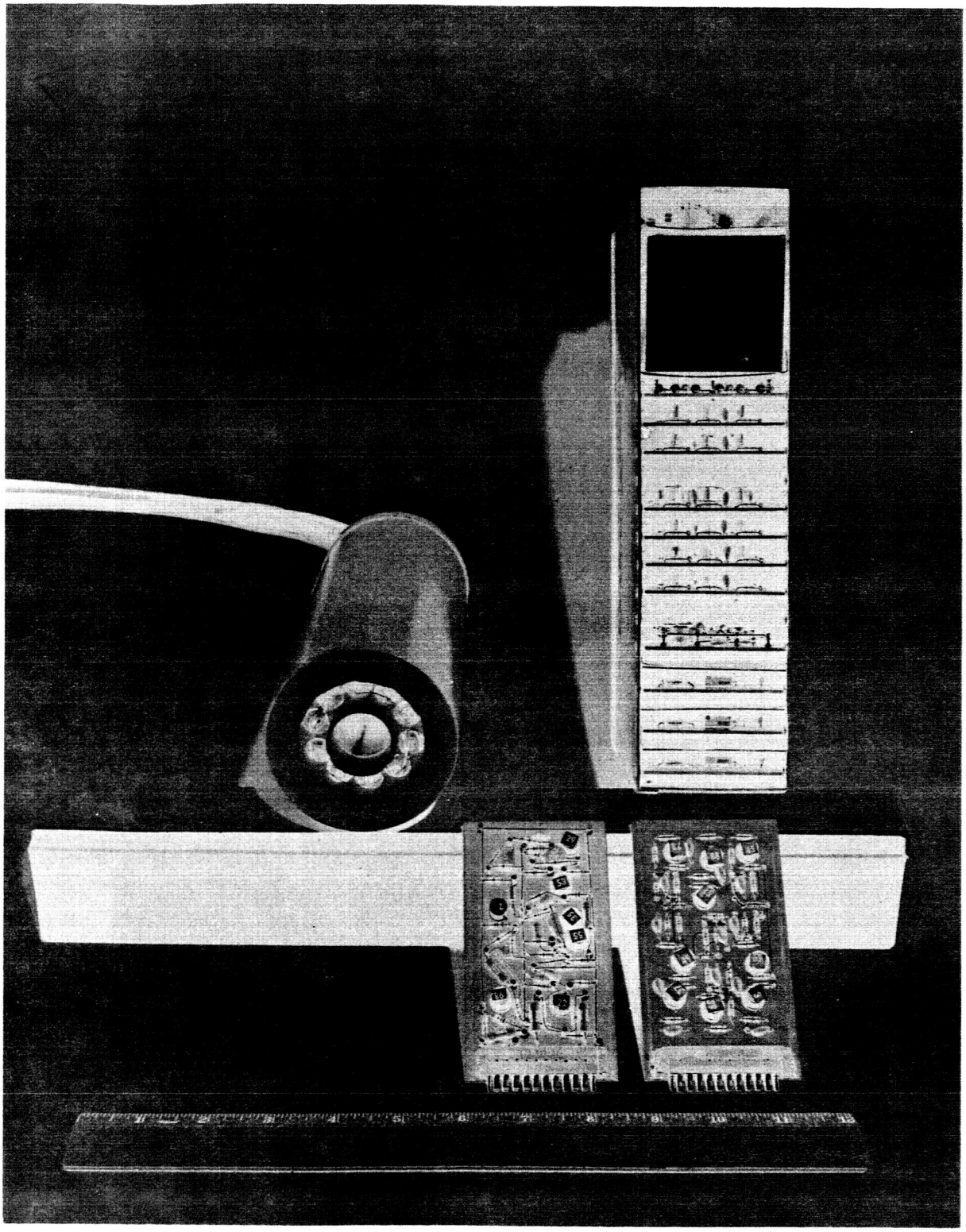

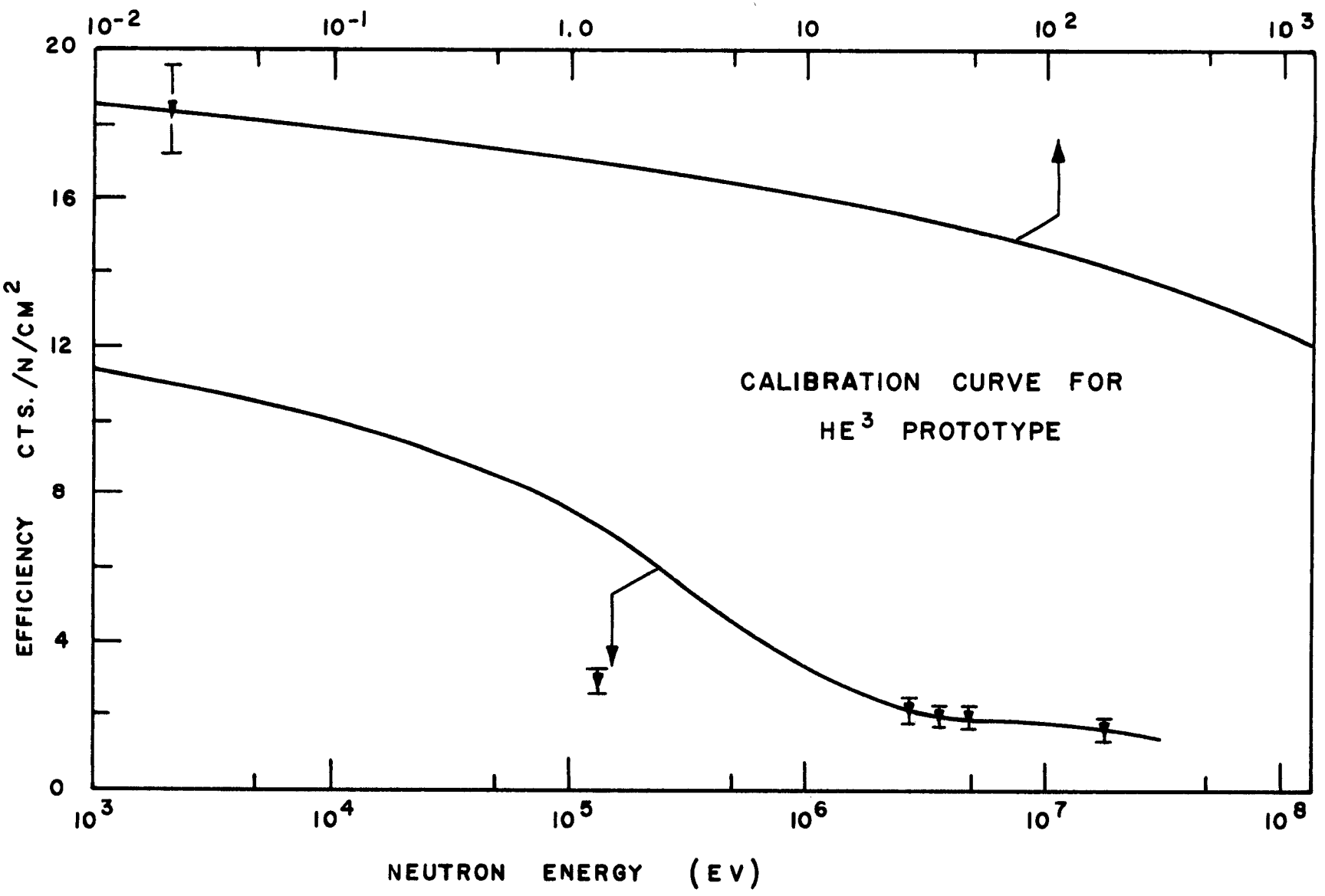
10-2
10-1
1.0
10
10 2
10 3
20
16
12
8
4
0
EFFICIENCY CTS./N/CM 2
CALIBRATION CURVE FOR
HE 3 PROTOTYPE
10 3
10 4
10 5
10 6
10 7
10 8
NEUTRON ENERGY (EV)

FIG. 15

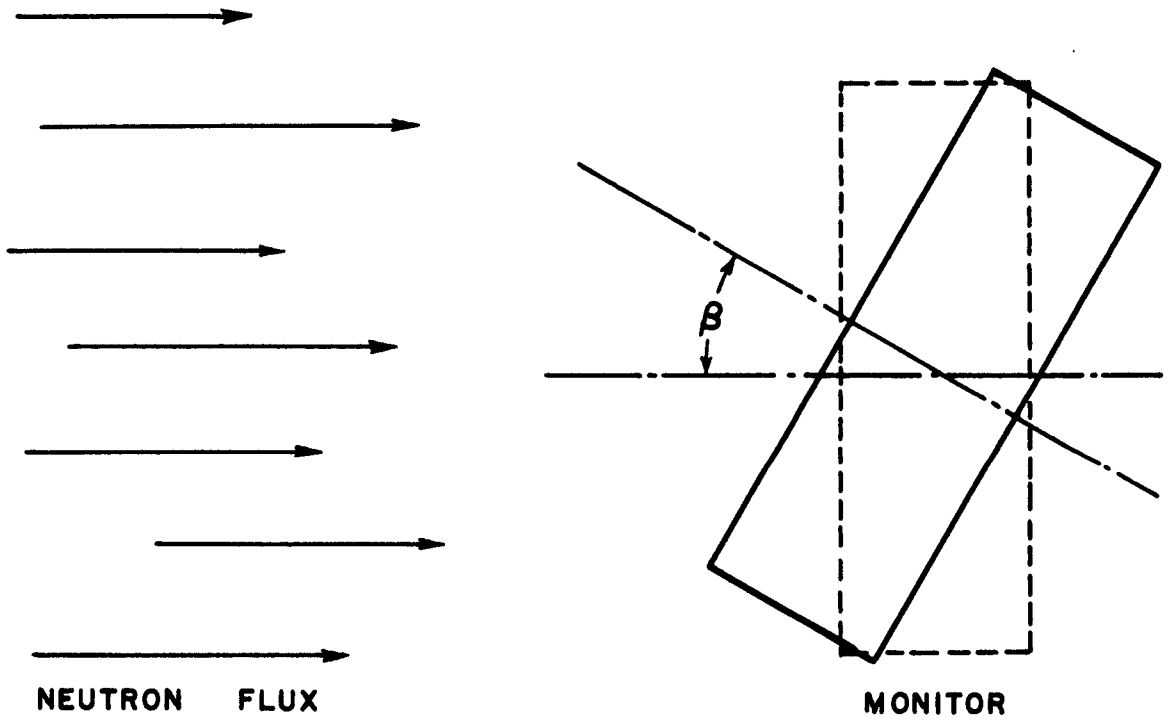

MEASURING ANGULAR DEPENDENCE

FIG. 16

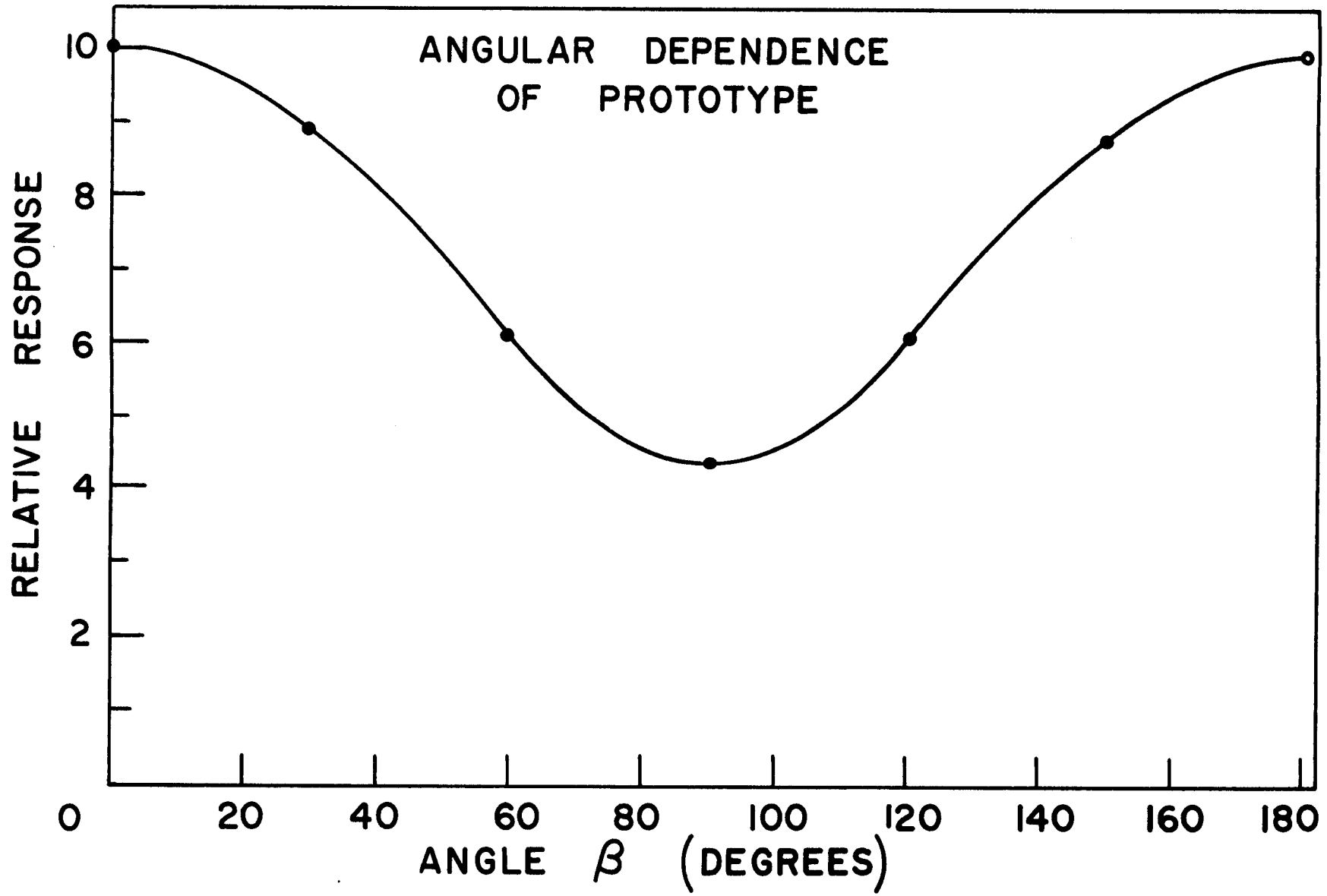
ANGULAR DEPENDENCE
OF PROTOTYPE
RELATIVE RESPONSE
10
8
6
4
2
0
20
40
60
80
100
120
140
160
180
ANGLE β (DEGREES)

FIG. 17

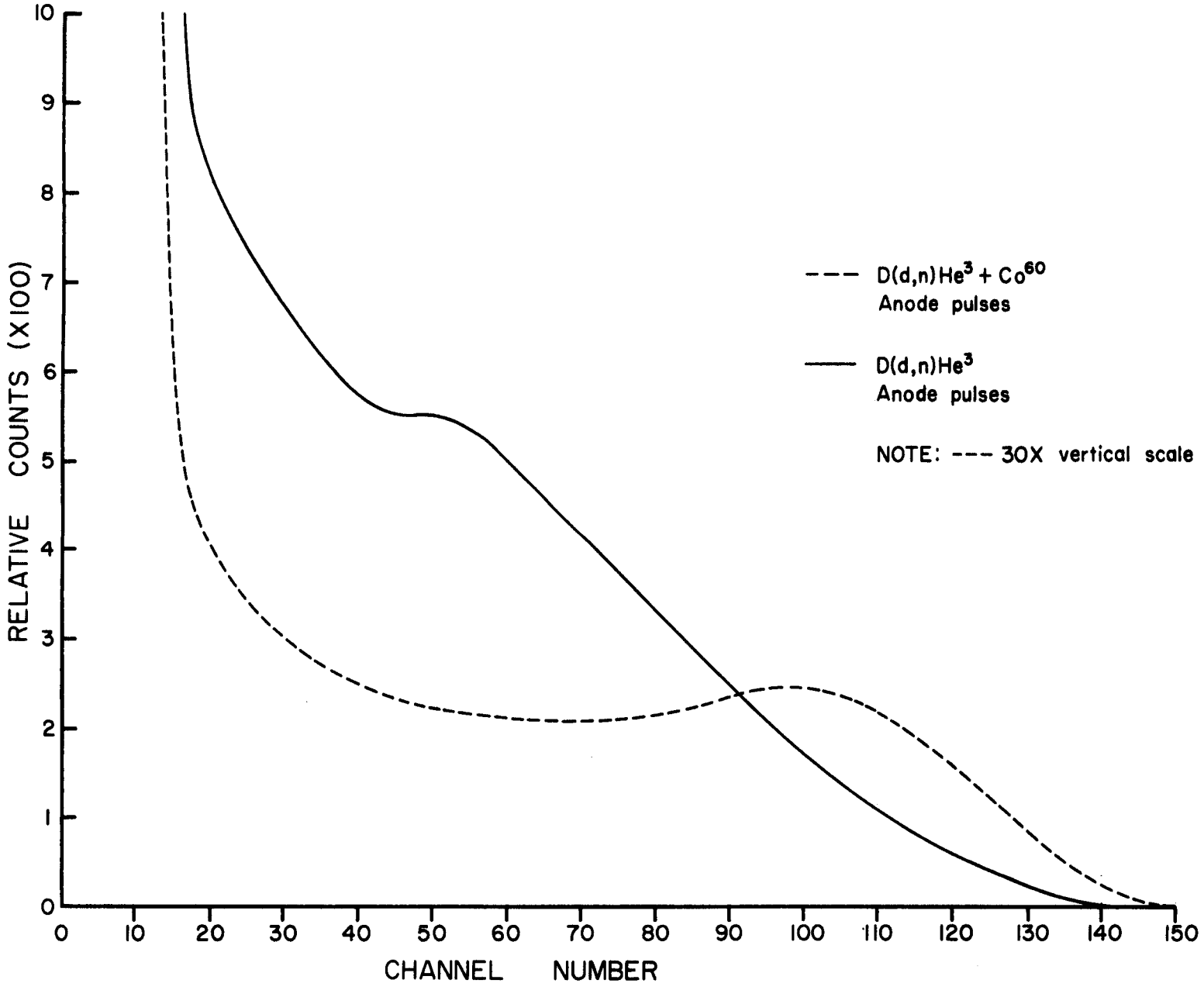
RELATIVE COUNTS (X100)
CHANNEL NUMBER
0
1
2
3
4
5
6
7
8
9
10
0
10
20
30
40
50
60
70
80
90
100
110
120
130
140
150
--- D(d,n)He3 + Co60
Anode pulses
—— D(d,n)He3
Anode pulses
NOTE: --- 30X vertical scale

FIG. 18A

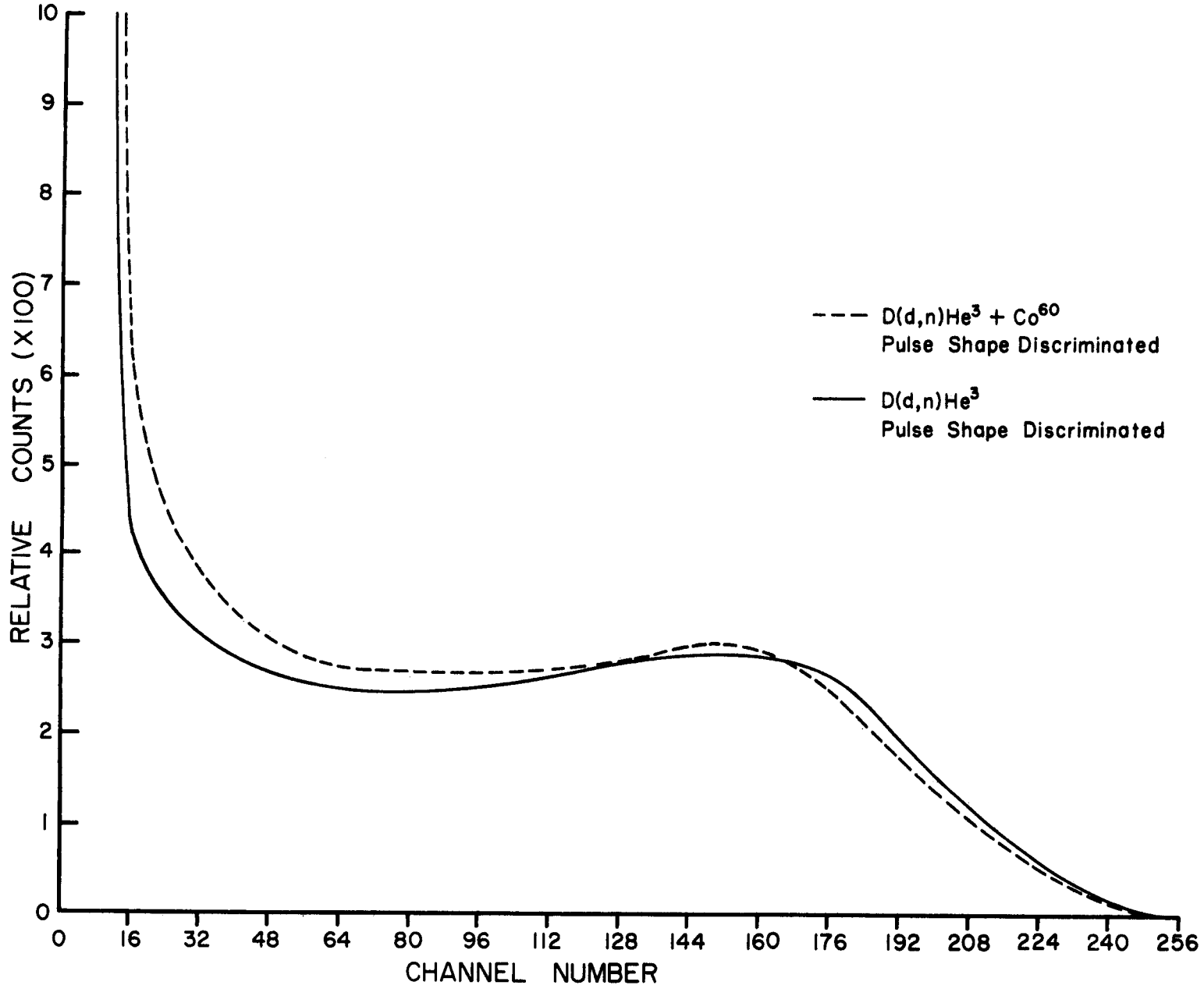
RELATIVE COUNTS (X100)
0
1
2
3
4
5
6
7
8
9
10
0
16
32
48
64
80
96
112
128
144
160
176
192
208
224
240
256
CHANNEL NUMBER
D(d,n)He3 + Co60
Pulse Shape Discriminated
D(d,n)He3
Pulse Shape Discriminated

FIG. 18B

Appendix A

Schematic Diagrams of Electronic Circuits for the Prototype Space Neutron Monitor

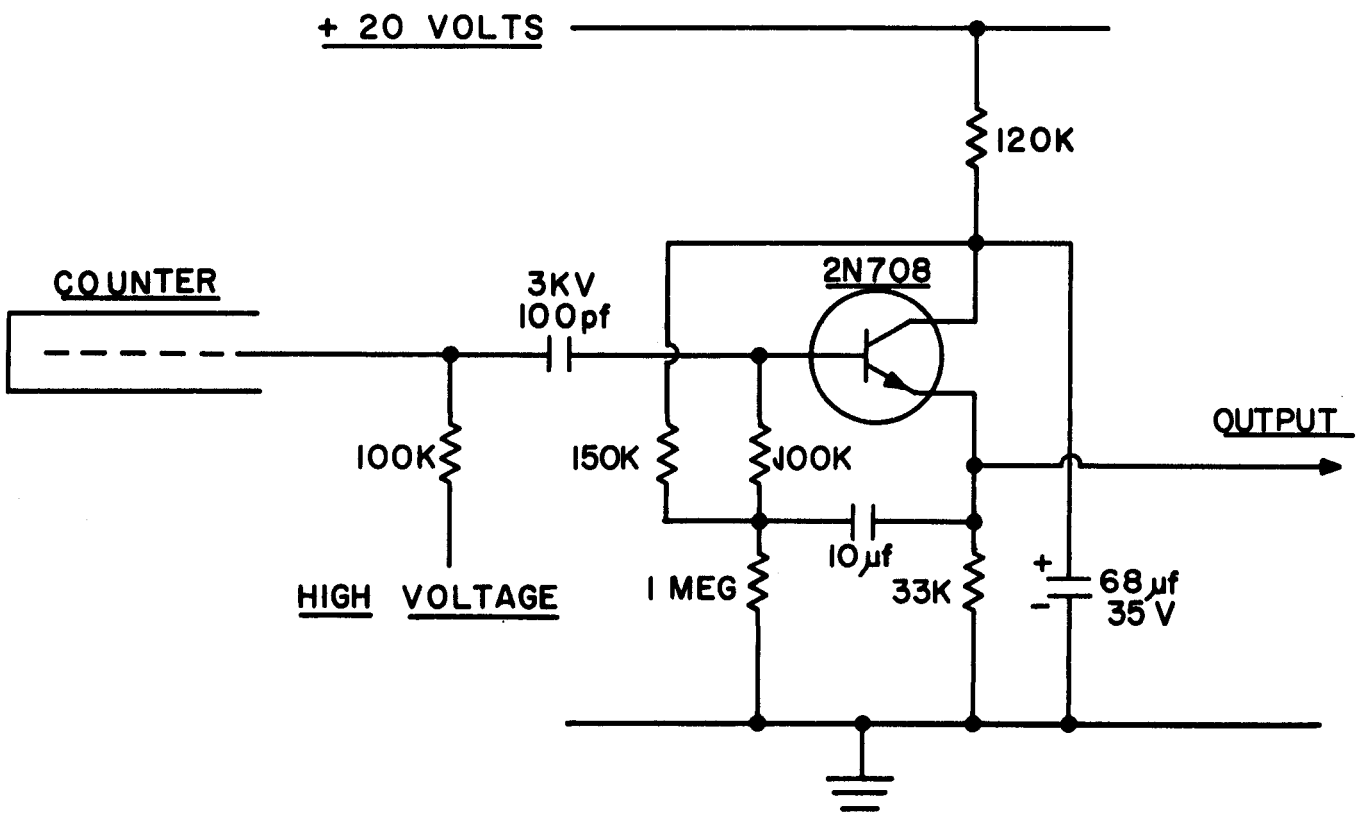

PREAMPLIFIER

FIG. A1

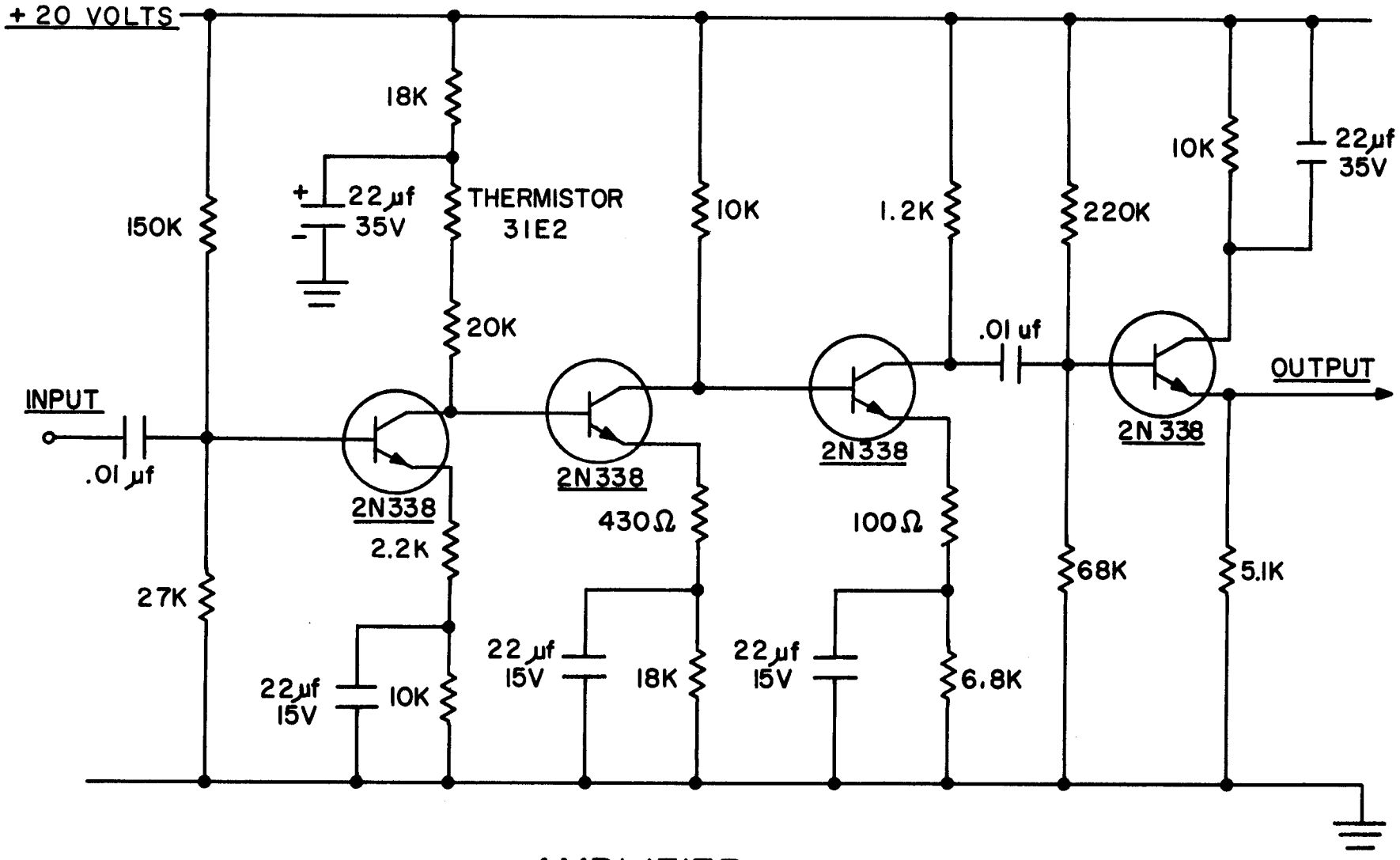

AMPLIFIER

FIG. A2

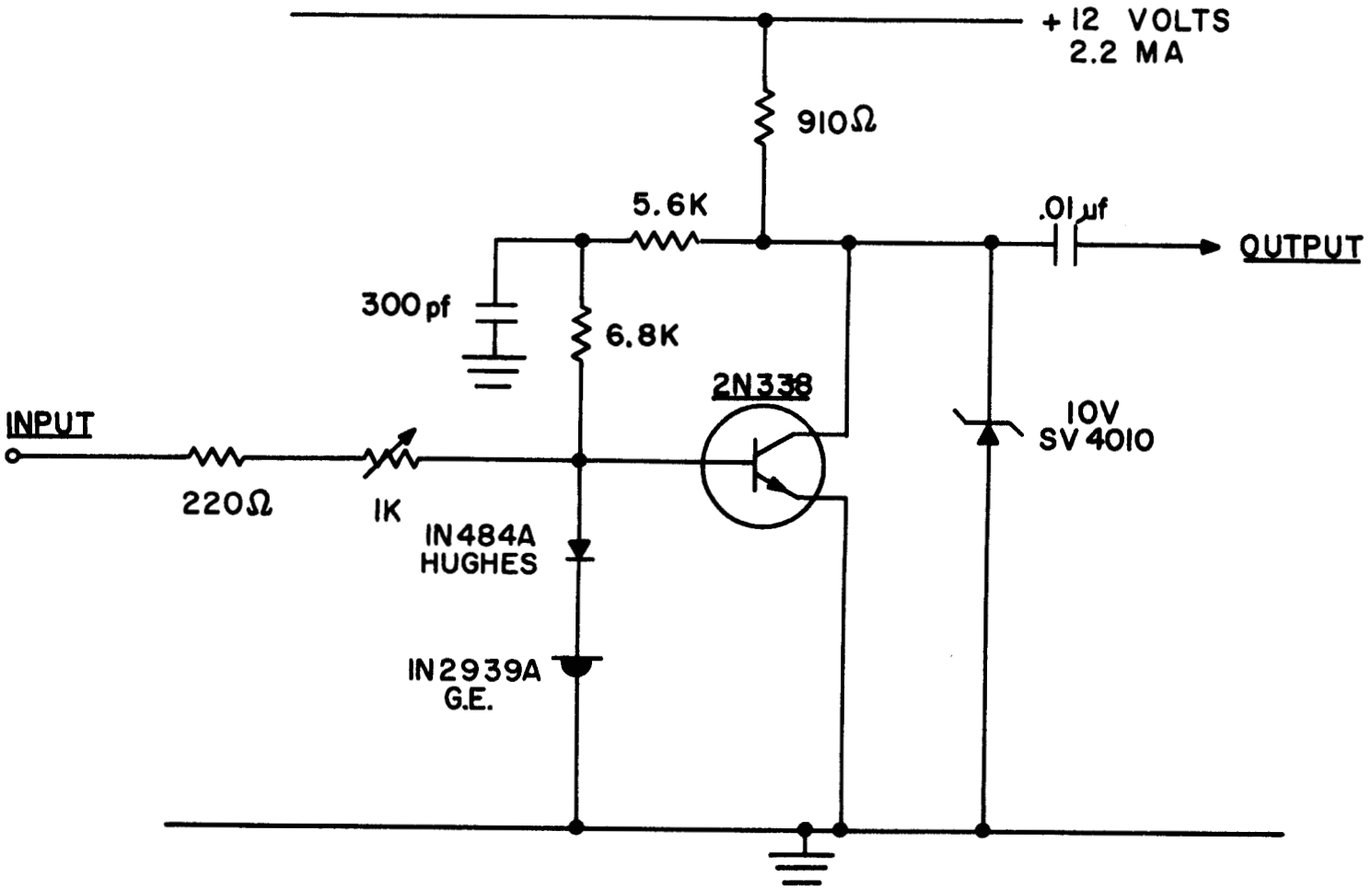

PULSE DISCRIMINATOR

FIG. A3

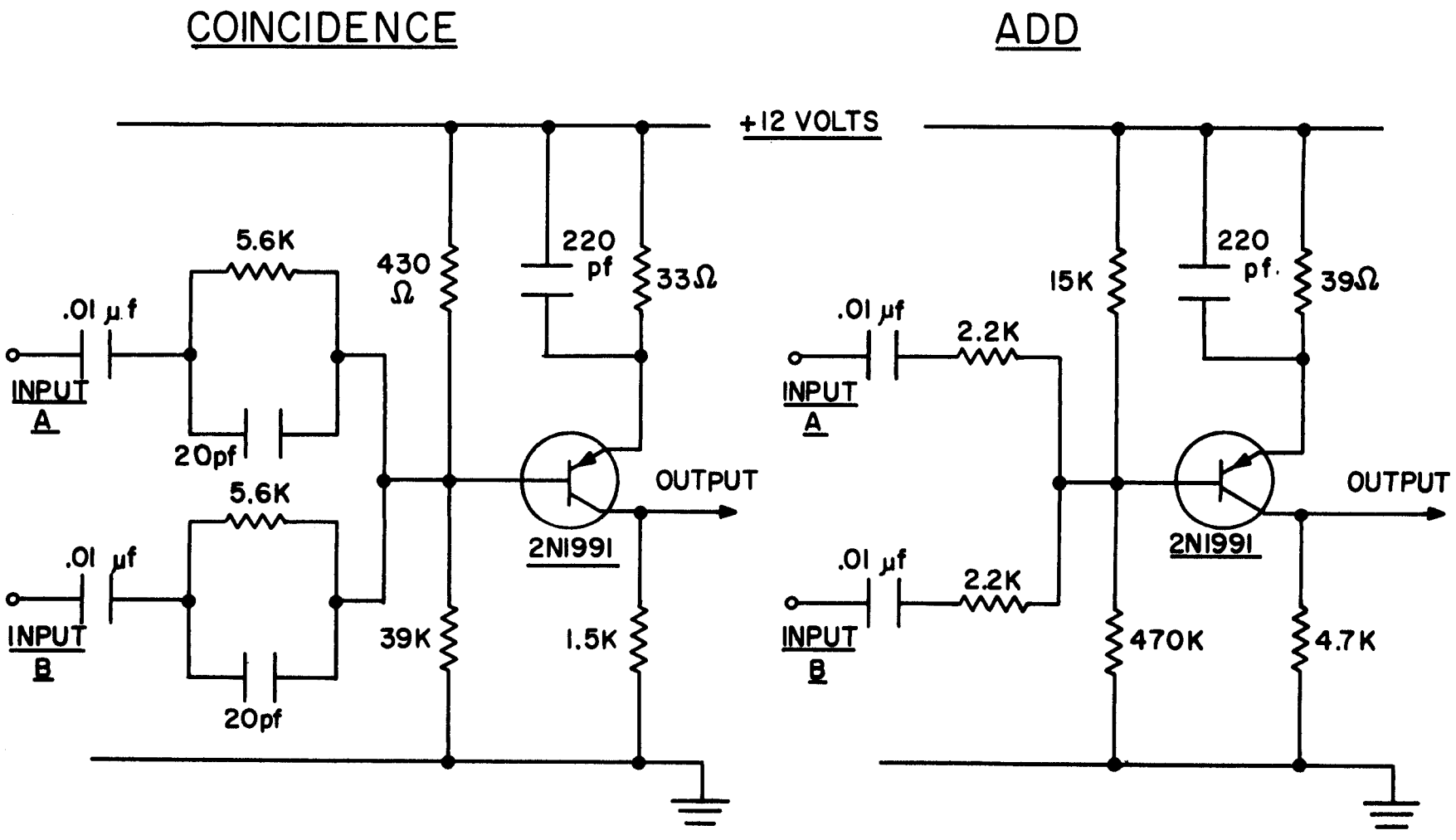

LOGIC CIRCUITS

FIG. A4

ANTI-COINCIDENCE

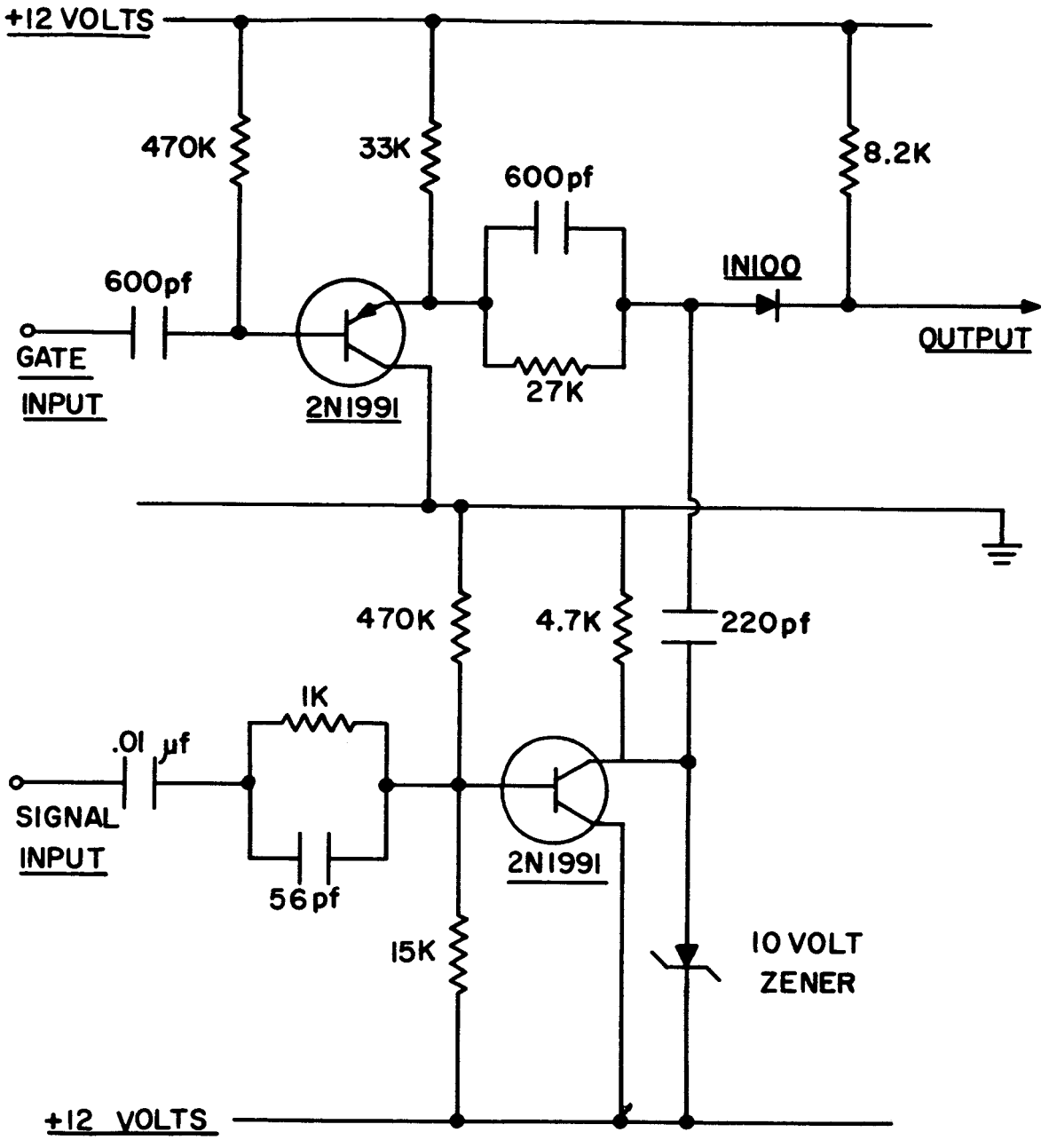

LOGIC CIRCUITS

FIG. A5

200 μSEC MONOSTABLE & INVERTER

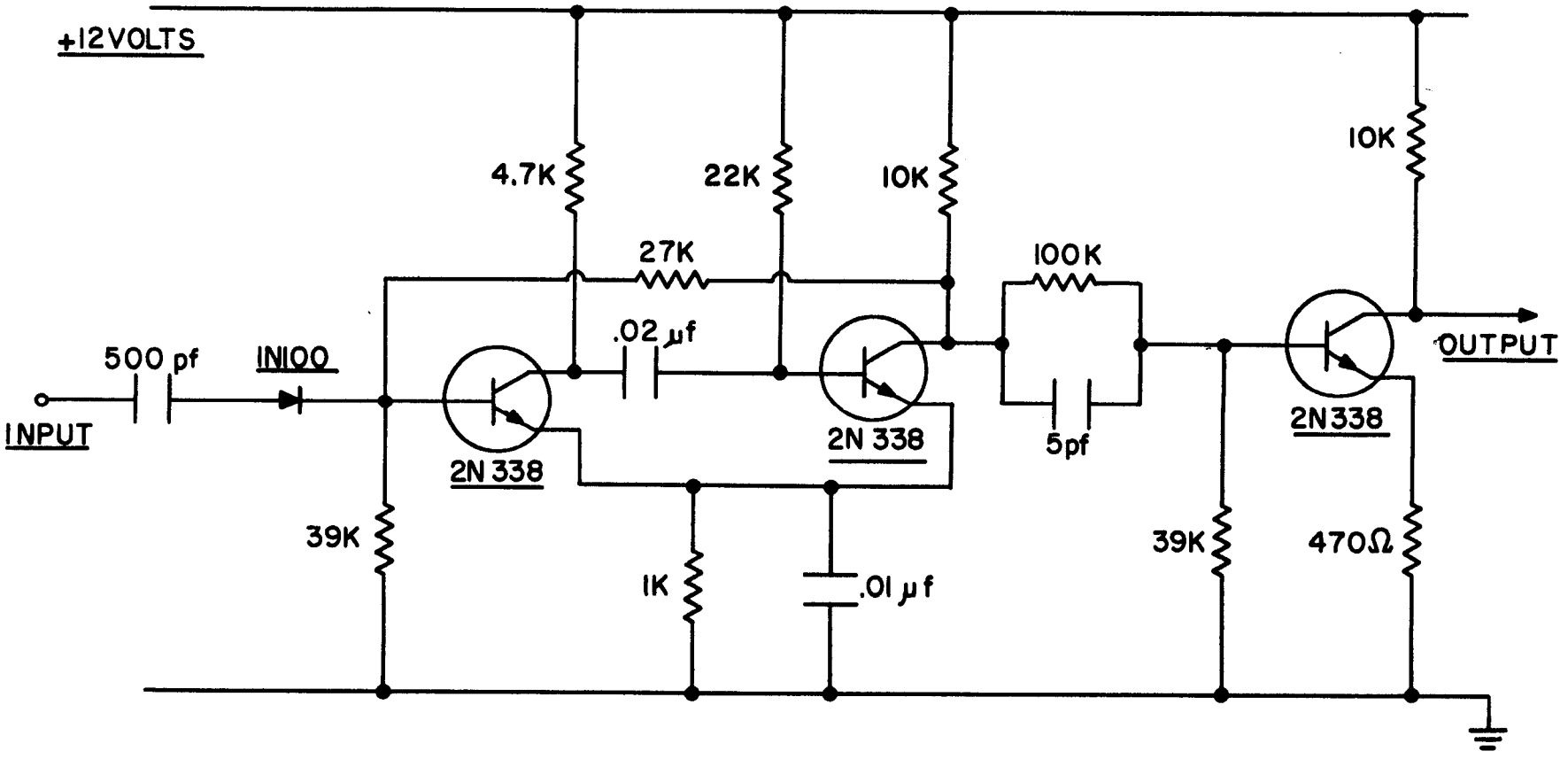

LOGIC CIRCUITS

FIG. A6

Appendix B

LiI Neutron Detector

A neutron detector constructed for comparison with the He^3 and BF_3 proportional counters consisted of a Li^6I (Eu) scintillator (Harshaw Chemical Corporation), encased in a plastic scintillator, P' - Diphenylstilbene, manufactured by Pilot Chemicals, Inc., and designated as Pilot B. This detector was developed following the suggestion of E. L. Chupp, who directed R. L. Colburn in this investigation. The phoswich assembly is shown in Fig. B-1. The Li^6I (Eu) crystal is 2.235 in. diameter and 2 mm. thick, and enclosed in a metal housing on two sides with a glass cover on the front side. The Pilot B scintillator was machined from stock and painted on all outside surfaces, except the one coupled to the photomultiplier, with a special reflector paint manufactured by Nuclear Enterprises, Ltd. All optical couplings were made with Dow Corning XC-2-0057.

The Pilot B scintillator serves two purposes (see Section V): (1) for discrimination against neutron production in the detector by charged particles, and (2) as a moderator to slow down energetic neutrons, thereby increasing the efficiency for detection of higher energy neutrons. The charged particle discrimination occurs since the fast pulse produced in the plastic scintillator by the incident charged particle is used to derive a gate pulse which turns off the output of the neutron detection channel. An obvious disadvantage is that the recoil nuclei from elastic collisions in the scintillator-moderator will produce light pulses of comparable

magnitude to those in Li^6I. For neutron energies below 10 Mev this will not be a problem, because the relative light output pulse for identical energy losses in the scintillators is about twice as large for Li^6I (Eu) as it is for Pilot B. In addition, the resulting capture of slow neutrons by $H(\sigma \sim 0.3b)$ produces a pulse of 2.19 Mev. Such a pulse could occasionally trigger the gate circuit for charged particle discrimination, hence increasing the dead time of the detector array.

The response of the phoswich assembly to charged particles, gamma rays, and neutrons should be as follows:

1. Low-energy charged particles should lose all their energy in the plastic to produce a single fast pulse. If the resulting voltage pulse is above the threshold of the pulse shape discriminator, a gate pulse will be produced. For higher energy particles, able to penetrate both the plastic and LiI scintillators, a composite pulse will result. Since this pulse contains both a fast and a slow component, a gate pulse will also be produced. The exact energy threshold for charged particle detection was not determined.

2. Thermal neutrons may be captured in the plastic scintillator, and the resulting γ pulses may be large enough to produce a spurious gate signal. Only a very small fraction of the thermal neutrons would be expected to produce such gating signals.

3. Fast neutrons will be scattered in the plastic scintillator, and a series of fast pulses will be produced by the recoil protons. Such pulses, especially where the first recoil proton pulse is large, may result in self-gating, depending upon the threshold setting. The response of the phoswich assembly to such events must be carefully checked.

4. Even though the Plastic B and thin Li^6I scintillator have only a low efficiency for gamma rays, some difficulties with gamma rays may be encountered in the laboratory because most neutron sources have large gamma fluxes and some gamma radioactivity is always produced with the accelerator.

The pulse shape discriminator, the schematic diagram for which is shown in Fig. B-2, is based upon the design of Peterson and Nitardy (1961) for use with a NaI-plastic phoswich. In the experimental tests performed, a gate generator was constructed to provide a pulse to gate the pulse height analyser, a type RCL-256.

Four different experiments were made on the phoswich assembly: First, the optimum values were determined for the parameters C_1 and C_3 in the pulse shape discrimination circuit. Second, the response of the Pilot B scintillator to various energy neutrons was evaluated. Third, the response of the Li^6I scintillator was similarly determined. Fourth, the complete phoswich assembly was exposed to known fluxes of different energy neutrons.

The experimental set-up to determine the response characteristics of the scintillators to neutrons was essentially the same as used for the efficiency measurements on the space neutron monitor shown in Figs. 7 and 8. In all cases the optimum value of C_3 = 400 pf was used and the high voltage on the photomultiplier set at less than 1150 volts to avoid the possibility that gate pulses will be generated in the pulse shape discriminator for slow rise time input pulses.

In Figs. B-3 and B-4 are displayed the gated and ungated spectra from the Pilot B, the LiI and the phoswich assembly. It is evident that the phoswich assembly operates satisfactorily for 3 Mev neutrons because the gating removes the pulses in the range of channels 80-150. These pulses

correspond to proton recoil below the threshold for generating a gating pulse. The slight shift in the peak occurring at about channel 180-200 in the pulse height distributions in the Li^6I and phoswich assembly is due to differences in the optical path in the two cases. A similar voltage pulse height distribution was obtained for 5 Mev neutrons. However, with 14 Mev neutrons the pulse height distribution is quite different, as can be seen in Figs. B-5 and B-6. The phoswich assembly does not operate properly here because, first, the fast neutrons produce recoil nuclei in the plastic, which in turn generate light pulses as large as from the Li^6I, and second, the pulse shape discriminator is saturatang, i.e., for sufficiently large pulses from the plastic no gate pulse is generated. With saturation in the pulse shape discriminator occurring, it is not clear what fraction of the 14 Mev neutrons are being self-gated. Apparently, the pulse height discriminator is saturating because the counting rate is too high with no clipping of the ringing pulse generated in the plastic scintillator. An investigation is being made of the possibility of clipping this pulse to increase the counting rate for which the pulse height discriminator saturates.

The measured efficiencies of the phoswich assembly for different energy neutrons are approximately

E_n = thermal	3 Mev	14 Mev
9.0 cm^2	2.8	2.8 .

These were determined with the high voltage at 1100 V under the same experimental conditions as for the space neutron monitor.

To consider using this phoswich assembly for measurements of neutrons in space, the saturation effects in pulse shape discriminator, and the energy at which self-gating becomes predominate must be investigated thoroughly. Despite the more elaborate electronics the overall detector assembly is relatively simple and has an efficiency comparable to the He^3 neutron monitor. Further tests are planned on this detector with a possible balloon flight of a prototype.

PHOSWICH ASSEMBLY

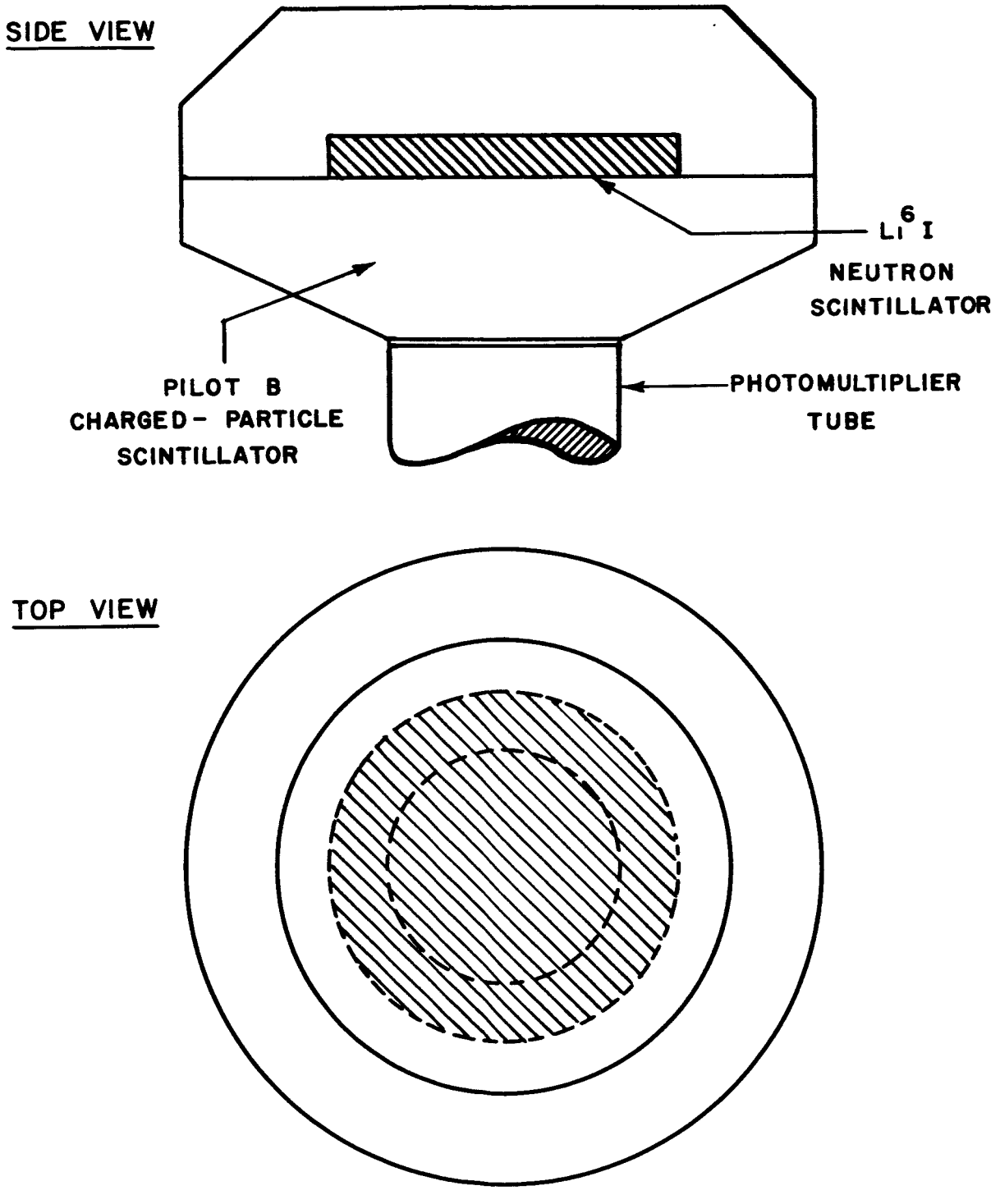

FIG. BI

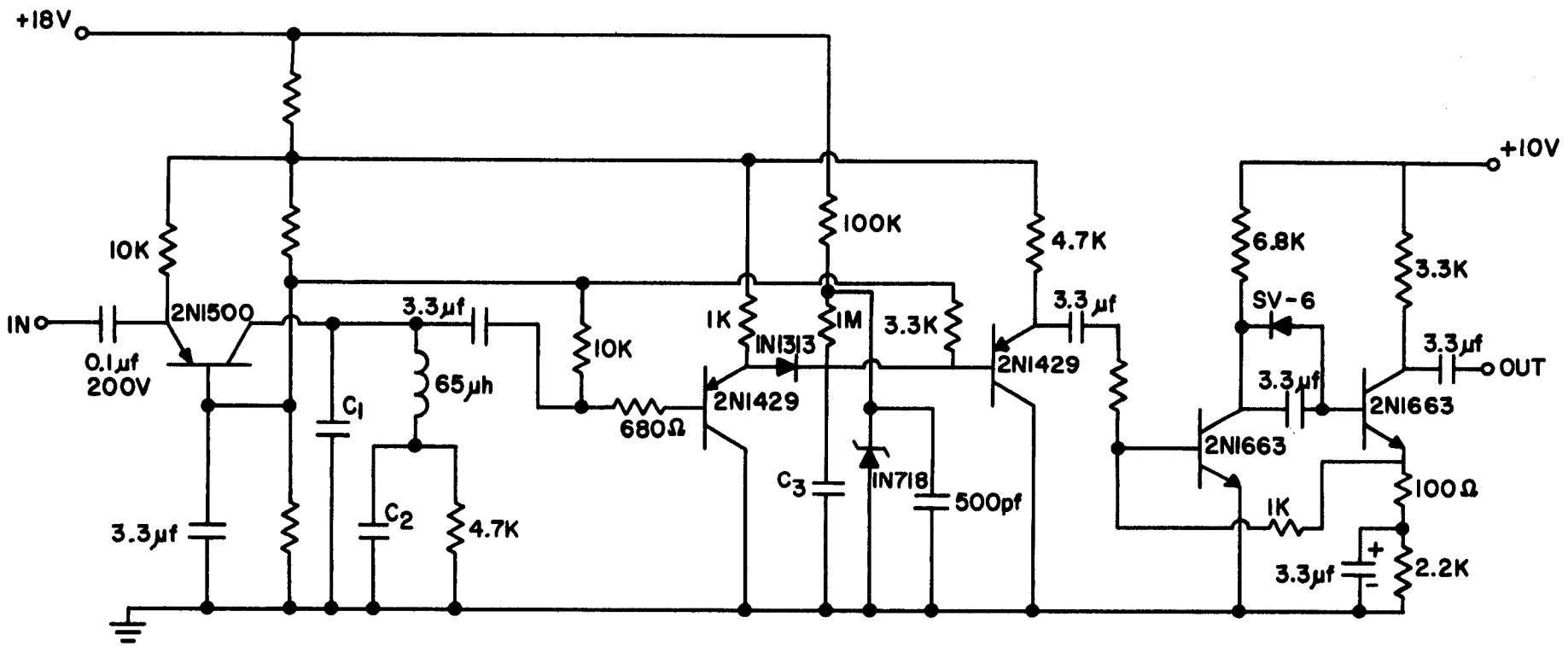

PULSE SHAPE DISCRIMINATOR

FIGURE 1

FIG. B2

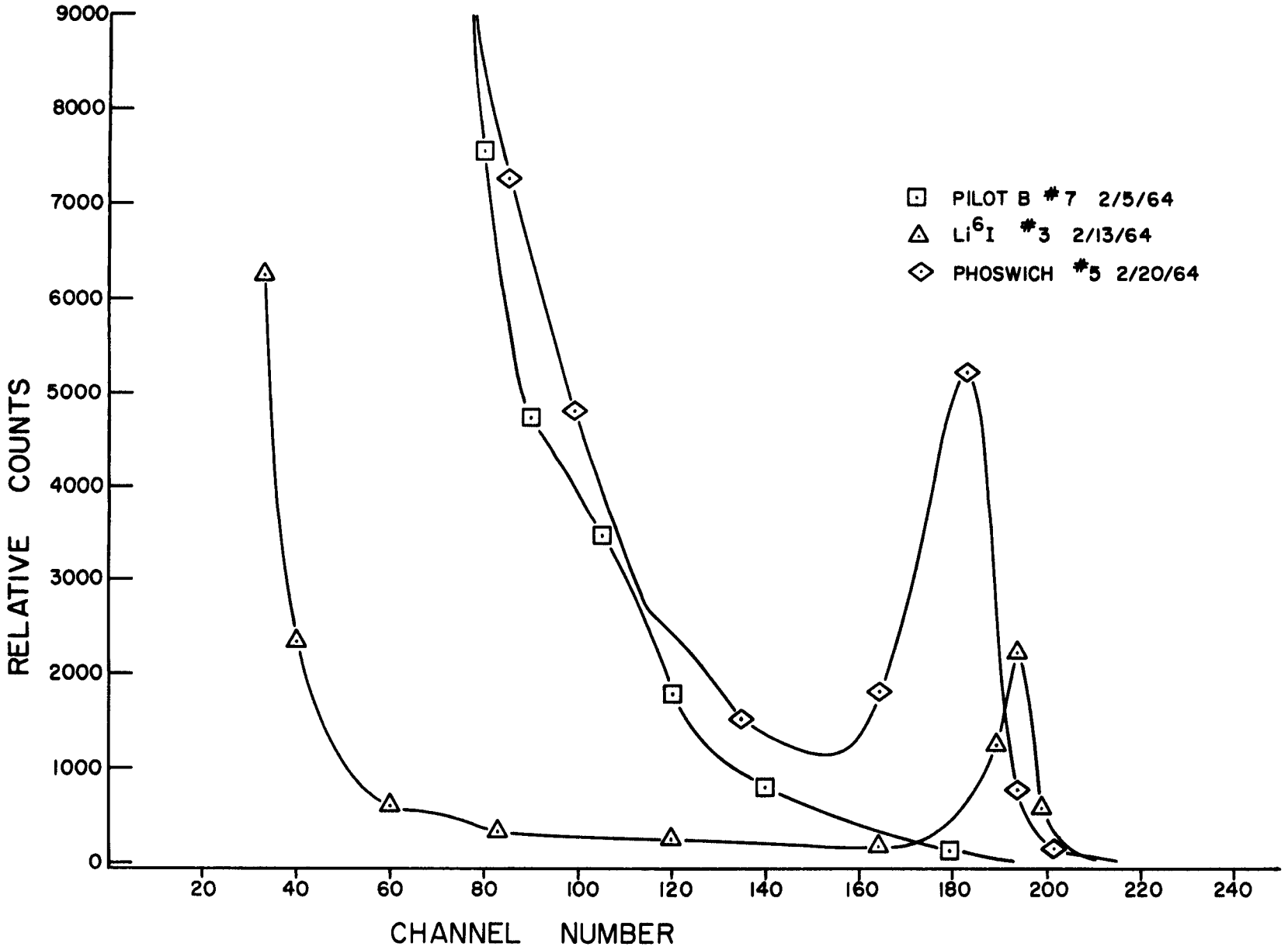
9000
8000
7000
6000
5000
4000
3000
2000
1000
0
RELATIVE COUNTS
20
40
60
80
100
120
140
160
180
200
220
240
CHANNEL NUMBER
PILOT B #7 2/5/64
Li6I #3 2/13/64
PHOSWICH #5 2/20/64

FIG. B3

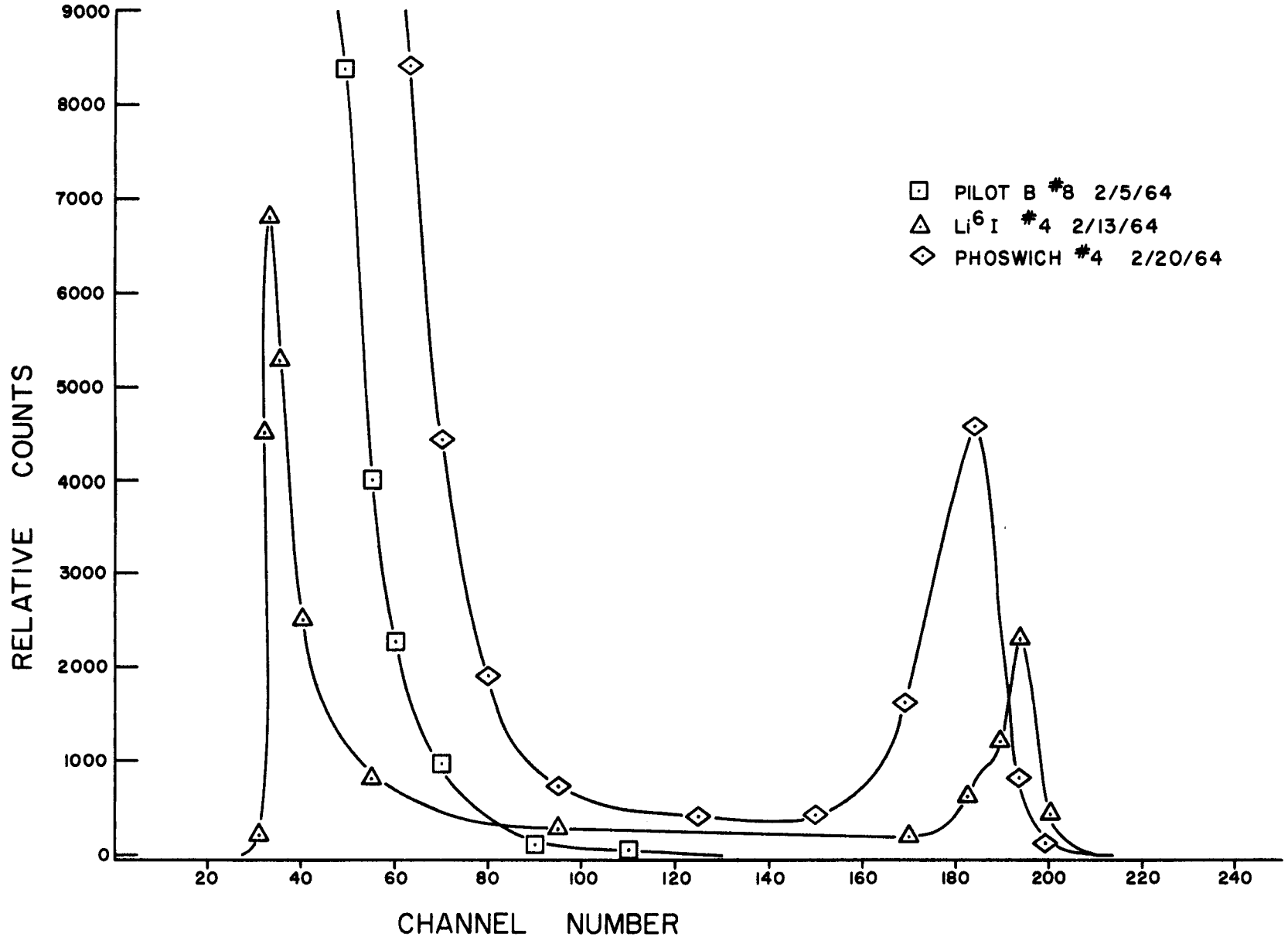
RELATIVE COUNTS
9000
8000
7000
6000
5000
4000
3000
2000
1000
0
20
40
60
80
100
120
140
160
180
200
220
240
CHANNEL NUMBER
PILOT B #8 2/5/64
Li6 I #4 2/13/64
PHOSWICH #4 2/20/64

FIG. B4

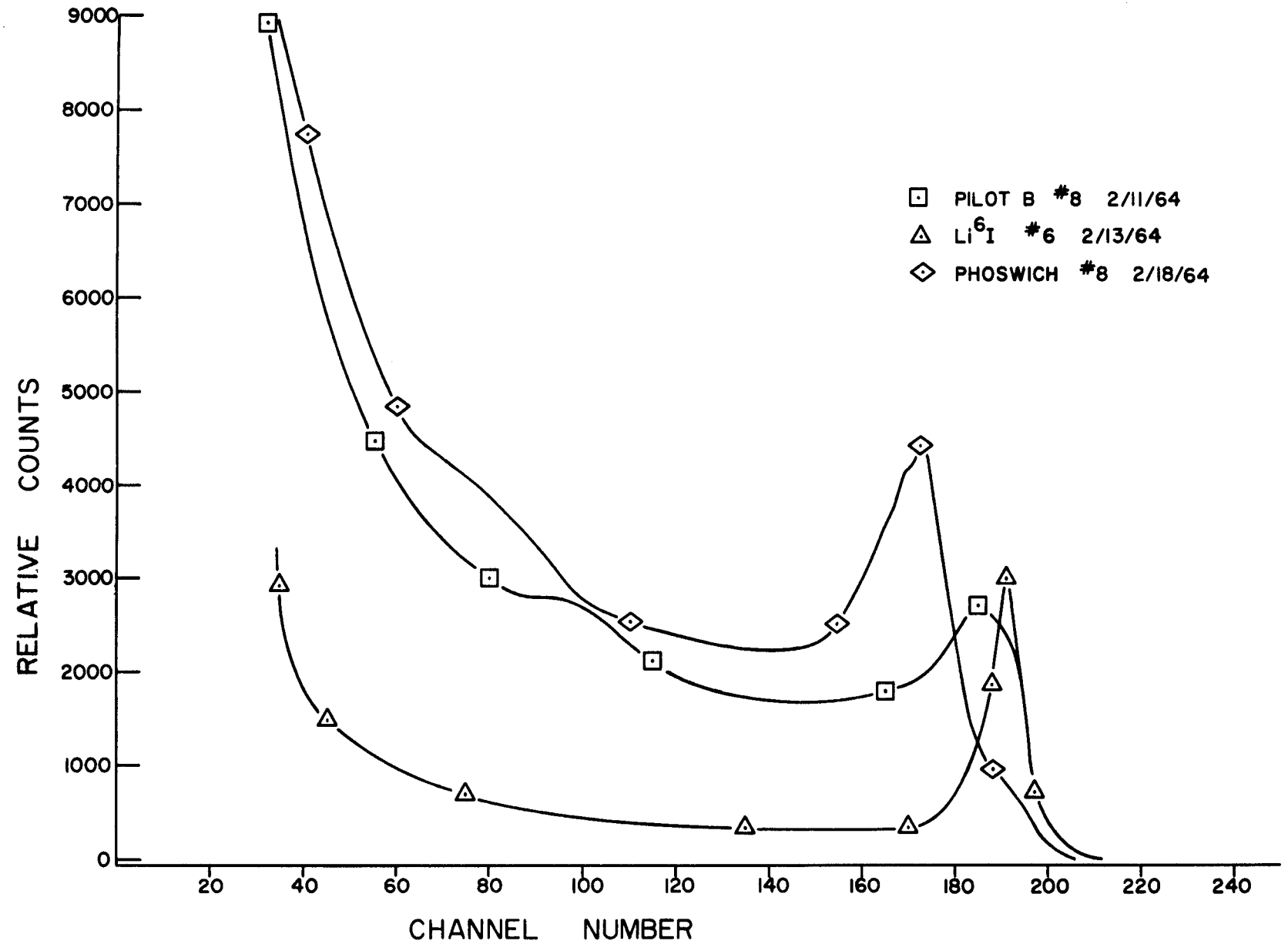
9000
8000
7000
6000
5000
4000
3000
2000
1000
0
RELATIVE COUNTS
20
40
60
80
100
120
140
160
180
200
220
240
CHANNEL NUMBER
PILOT B #8 2/11/64
Li6I #6 2/13/64
PHOSWICH #8 2/18/64

FIG. B5

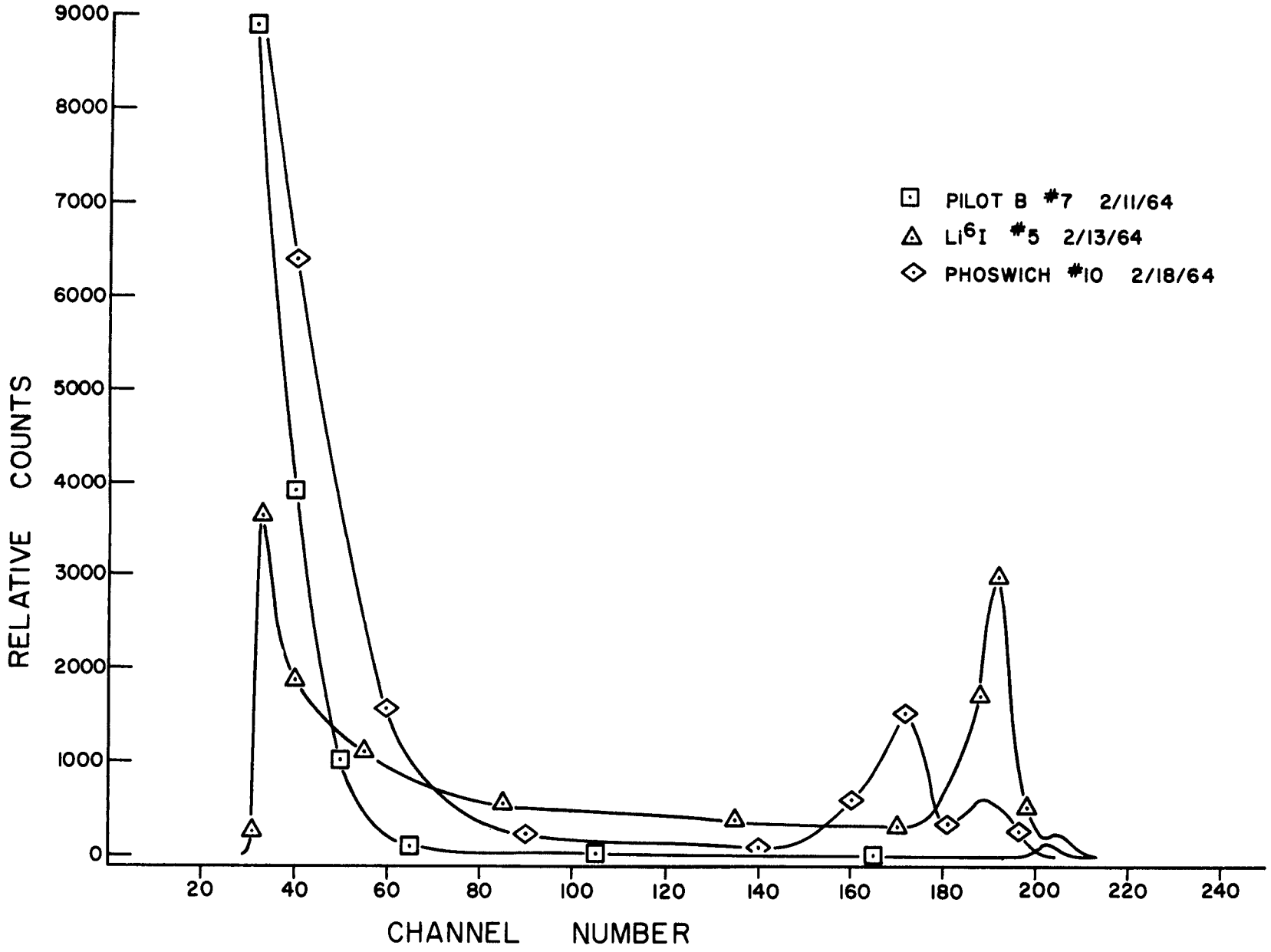
9000
8000
7000
6000
5000
4000
3000
2000
1000
0
RELATIVE COUNTS
20
40
60
80
100
120
140
160
180
200
220
240
CHANNEL NUMBER
PILOT B #7 2/11/64
Li6I #5 2/13/64
PHOSWICH #10 2/18/64

FIG. B6